
Exponentially Many Local Minima in Quantum Neural Networks

Xuchen You^{1,2} Xiaodi Wu^{1,2}

Abstract

Quantum Neural Networks (QNNs), or the so-called variational quantum circuits, are important quantum applications both because of their similar promises as classical neural networks and because of the feasibility of their implementation on near-term intermediate-size noisy quantum machines (NISQ). However, the training task of QNNs is challenging and much less understood. We conduct a quantitative investigation on the landscape of loss functions of QNNs and identify a class of simple yet extremely hard QNN instances for training. Specifically, we show for typical underparameterized QNNs, there exists a dataset that induces a loss function with the number of spurious local minima depending exponentially on the number of parameters. Moreover, we show the optimality of our construction by providing an almost matching upper bound on such dependence. While local minima in classical neural networks are due to non-linear activations, in quantum neural networks local minima appear as a result of the quantum interference phenomenon. Finally, we empirically confirm that our constructions can indeed be hard instances in practice with typical gradient-based optimizers, which demonstrates the practical value of our findings.

1. Introduction

Motivations. With the recent establishment of quantum supremacy (Arute et al., 2019; Zhong et al., 2020), the research of quantum computing has entered a new stage where near-term Noisy Intermediate-Scale Quantum (NISQ) computers (Preskill, 2018) become the important platform for demonstrating quantum applications. *Quantum Neural Networks (QNNs)* (e.g., Farhi et al. (2020; 2014)), or the

so-called variational quantum method (e.g., Peruzzo et al. (2014)), are the major candidates of applications that can be implemented on NISQ machines.

Typical QNNs replace classical neural networks (ClaNNs), which are just parameterized classical circuits, by quantum circuits with *classically parameterized unitary gates*. Instead of a classical mapping in ClaNNs from input to output, QNNs use a *quantum* one which could be very hard for classical computation to simulate (e.g., Harrow & Montanaro (2017)) and hence provide potential quantum speedups for machine learning tasks (e.g., see the survey by Biamonte et al. (2017) and by Harrow & Montanaro (2017) and examples in Schuld & Killoran (2019) and in Havlíček et al. (2019)). Moreover, given their quantum-mechanical nature, QNNs (or the variational quantum method) have also demonstrated huge promises in attacking problems in quantum chemistry and material science. Contrary to quantum supremacy tasks which serve only as a way to separate quantum and classical computational power but are not necessarily useful, Google has recently used the same machine to demonstrate the variational quantum method in calculating accurate electronic structures – an important task in quantum chemistry (Arute et al., 2020). Please see the survey (Benedetti et al., 2019) for more recent exciting developments of QNNs.

Similar to the classical case, the success of QNN applications will critically depend on the effectiveness of the training procedure which optimizes a *loss function* in terms of the *read-outs* and the *parameters* of QNNs for specific applications. The design of effective training methods has been under intense investigation both empirically and theoretically for ClaNNs. Moreover, understanding the landscape of the loss functions and designing corresponding training/optimization methods have recently emerged as a principled approach to tackle this problem: (Auer et al., 1996; Safran & Shamir, 2018; Yun et al., 2018; Ding et al., 2019; Venturi et al., 2018) showed the existence of spurious local minima for ClaNNs; In turn, (Kawaguchi, 2016; Du & Lee, 2018; Soudry & Carmon, 2016; Nguyen & Hein, 2017; Li et al., 2018) characterized conditions for benign landscapes in terms of choice of activation, loss function and (over)-parameterization, providing insights on the design of ClaNNs and motivating explanations to the success of gradient descent in training ClaNNs in certain scenarios

¹Joint Center for Quantum Information and Computer Science, University of Maryland ²Department of Computer Science and Institute for Advanced Computer Studies, University of Maryland. Correspondence to: X.You <xyou@umd.edu>, X.Wu <xwu@cs.umd.edu>.

(Jacot et al., 2018; Arora et al., 2019; Du et al., 2019); And training methods beyond simple variants of gradient descent have been devised for training with guarantees (Goel et al., 2017; Goel & Klivans, 2019; Zhong et al., 2017; Du & Goel, 2018).

Much less has been understood for QNNs. Most of the study of QNNs takes a trial-and-error approach by empirically comparing the performance of standard classical optimizers on training QNNs’ loss functions (Benedetti et al., 2019). It has been observed empirically that training QNNs could be very challenging due to the *non-convex* nature of the corresponding loss functions (e.g., Wang et al. (2020; 2018)). However, these empirical studies are unfortunately restricted to small cases due to the limited access to quantum machines of reasonable sizes and the exponential cost in simulating them classically.

A theoretical study on the training of QNNs would be more *favorable* and *scalable* given the limit on empirical study. Indeed, a handful of such theoretical progress has been made. One prominent result is that random initialization of parameters will lead to vanishing gradients for much smaller size QNNs than ClaNNs (McClean et al., 2018) and hence pose one unique training difficulty for QNNs. Most of the remaining theoretical results are about special cases of QNNs such as *quantum approximate optimization algorithms* (QAOA) (e.g., Farhi et al. (2014); Farhi et al. (2019)) and extremely over-parameterized cases (e.g., Rabitz et al. (2004); Russell et al. (2016); Kiani et al. (2020)).

In this paper, we conduct a quantitative investigation on the landscape of loss functions for QNNs as a way to study their training issue. In particular, we are interested in understanding the properties of local minima of loss functions, such as, (1) the number of local minima depending on the architecture of QNNs, and (2) whether these local minima are *benign* or *spurious* ones, meaning that they are either close to the global minima or saddle points that can be escaped, or they are truly bad local minima that will hinder the training procedure. We are also motivated by the observation that QNNs share some similarity with linear neural networks without non-linear activation layers (Kawaguchi, 2016) or one-hidden layer neural networks with quadratic activation (Du & Lee, 2018) that are both known to have only benign local minima. The similarity is due to the fact that quantum mechanics underlying QNNs has a linear algebraic formulation similar to the linear part of ClaNNs. (Details in Section 2.) It is hence natural to wonder whether the local minima of QNNs could share these nice properties.

Contributions. Contrary to our original hope, we turn out to identify a class of *simple yet extremely hard* instances of QNNs for the training. Despite the similarity between QNNs and linear classical neural networks, we demonstrate that *spurious* (or *sub-optimal*) local minima do appear in

QNNs and provide a quantitative characterization of the possible number of them. We focus on QNNs with the commonly used *square loss* function under a practical range of the number of parameters (or gates). Specifically, we identify a general condition of under-parameterized QNNs, which we refer to as QNNs *with linear independence*. We show for such QNNs, a dataset can be constructed such that the number of spurious local minima scales *exponentially* with the number of parameters. It demonstrates that QNNs behave quite differently from linear neural networks (e.g., Kawaguchi (2016)) but share the feature of neurons with *non-linear* activation functions (e.g., Auer et al. (1996)). This conceptual paradox could be explained by one central phenomenon of quantum mechanics behind QNNs called *interference*. We observe that interference replaces the role of non-linear activation in creating bad local minima for QNNs. (Section 3)

We investigate further and prove that typical under-parameterized QNNs are indeed *with linear independence*. This indicates that for almost all under-parameterized QNNs, there is a dataset where training with simple variants of gradient-based methods is hard. (Section 4)

Moreover, we show our construction is almost *optimal* in terms of the dependence of the number of local minima on the number of parameters, by developing an almost matching upper bound. This upper bound also demonstrates a sharp separation between QNNs and ClaNNs: For ClaNNs, provided an arbitrary number of training samples, the number of local minima could be unbounded, and hence won’t be upper bounded by any function of the number of parameters (Auer et al., 1996). (Section 5)

Finally, we perform numerical experiments on concrete QNN instances with typical optimizers, and empirically confirm that our constructions can indeed be hard instances in practice. These experiments strengthen the value of our theoretical findings on the practical end. (Section 6)

It is worthwhile mentioning that our investigation on the landscape of loss functions has a direct implication on the hardness of gradient-based methods. While it does not rule out the possibility of efficient non-gradient-based training, there are no obvious solutions to the efficient training for our constructions. Identifying such training methods would be very interesting.

Related work. There are only a few previous studies on the training of QNNs, each of which has targeted at some specific parameter range for QNNs. The observation of vanishing gradients for random initialization of QNNs (McClean et al., 2018) provides hard QNN instances for training, which, however, still require many layers to demonstrate the difficulty of training in practice. Our constructions are based on a general condition which includes simple special

cases like 1-layer QNNs that are already able to demonstrate QNNs' training difficulty.

Another line of work (Rabitz et al., 2004; Russell et al., 2016; Kiani et al., 2020) considers the extremely over-parameterized QNN cases. Specifically, when the number of parameters is comparable to the dimension of the underlying quantum system and the quantum *controllability* condition can be established, all local minima of QNNs' loss functions will become global (Rabitz et al., 2004; Russell et al., 2016). This theoretical prediction has also been observed empirically (Kiani et al., 2020). However, as the dimension of quantum systems grows *exponentially* with the number of qubits, this over-parameterized case can hardly be realistic for any QNN of reasonable size.

2. Preliminaries

Supervised learning. The goal of supervised learning is to identify a mapping from the feature space \mathcal{X} to the label space \mathcal{Y} , given a training set $\{(\mathbf{x}_i, y_i)\}_{i=1}^m \subset (\mathcal{X} \times \mathcal{Y})^m$ of m samples of *feature vectors* and *labels*. A common practice to find a mapping based on a training set is through empirical risk minimization (ERM), finding a mapping that best align with the training sample with respect to a specific loss function $l: \mathcal{Y} \times \mathcal{Y} \rightarrow \mathbb{R}$. Let \hat{y}_i be the prediction of a certain mapping given \mathbf{x}_i . The goal of ERM is to find the mapping that minimizes the average loss $\frac{1}{m} \sum_{i=1}^m l(\hat{y}_i, y_i)$. Throughout this paper we will consider square loss $l(\hat{y}, y) = (\hat{y} - y)^2$.

Classical neural networks (ClnNs). Neural networks are parameterized families of mappings, widely considered for practical problems. Typical feed-forward neural networks are parameterized by a sequence of matrices $\{\mathbf{W}_i\}_{i=1}^t$, such that $\mathbf{W}_i \in \mathbb{R}^{d_i \times d_{i-1}}$, with $d_t = 1$ and d_0 is the same as the dimension of the feature space \mathcal{X} . For feature vector \mathbf{x} , the output \hat{y} of the neural network is

$$\hat{y} = \mathbf{W}_t \sigma(\mathbf{W}_{t-1} \sigma(\cdots \sigma(\mathbf{W}_1 \mathbf{x}) \cdots)), \quad (1)$$

where $\sigma(\cdot)$ denotes an element-wise activation on the output of each layer. (See Figure 1.) Linear neural networks (Kawaguchi, 2016) is one special example where σ is the identity mapping $\sigma(w) = w$: $\hat{y} = \mathbf{W}_t \mathbf{W}_{t-1} \cdots \mathbf{W}_1 \mathbf{x}$. Another example is one-hidden layer neural networks with quadratic activation $\sigma(w) = w^2$ (Du & Lee, 2018), where the output $\hat{y} = \mathbf{x}^T \mathbf{W}_1^T \mathbf{W}_1 \mathbf{x}$. Given the training set $\{(\mathbf{x}_i, y_i)\}_{i=1}^m$, the empirical risk minimization with square loss solves the optimization problem:

$$\min_{\mathbf{W}_1} \frac{1}{m} \sum_{i=1}^m (\mathbf{x}_i^T \mathbf{W}_1^T \mathbf{W}_1 \mathbf{x}_i - y_i)^2 \quad (2)$$

A common choice of $\sigma(\cdot)$ is non-linear activation such as Relu or Sigmoid. These activations introduce *non-linearity*

which is the source of spurious local minima in neural networks (Kawaguchi, 2016; Auer et al., 1996).

Quantum neural networks. QNNs share the layered structure (Figure 1) where a linear transformation \mathbf{U}_i is applied on the output of the previous layer, however, with the following differences:

(1) *Input.* The inputs to ClnNs are feature vectors. Yet for QNNs, a feature vector \mathbf{x} is first encoded into a quantum state $\rho_{\mathbf{x}}$ then fed to the quantum circuits. We are not restricted to specific encoding scheme (e.g., (Mitarai et al., 2018; Benedetti et al., 2019; Lloyd et al., 2020)). For technical convenience, we will directly work with a set of m samples of *quantum encoding* and *labels* $\mathcal{S} = \{(\rho_i, y_i)\}_{i=1}^m$ where ρ_i encodes the information of \mathbf{x}_i .

(2) *Linear Transformation & Parameterization.* The linear transformations $\{\mathbf{W}_i\}_{i=1}^t$ in ClnNs could be general matrices, whereas the corresponding $\{\mathbf{U}_i\}_{i=1}^t$ in QNNs must be unitaries. Moreover, although $\{\mathbf{U}_i\}_{i=1}^t$ can be efficiently implemented by quantum machines, their classical representations are matrices of exponential dimension in terms of the system size (e.g., the number of qubits in QNNs). This makes classical simulation of QNNs extremely expensive and also makes the parameterizations of $\{\mathbf{U}_i\}_{i=1}^t$ different from the straightforward parameterizations of $\{\mathbf{W}_i\}_{i=1}^t$ (explained below).

(3) *Output.* Contrary to ClnNs, one needs to make a quantum *measurement* to read information from QNNs (explained below). While there exist more advanced models of QNNs with additional nonlinearity, we consider the most basic QNNs, where the measurements are the only source of slight non-linearity allowed by quantum mechanics, which as we will see won't necessarily create bad local minima for the training. Note further there is no direct counterpart of classical non-linear activation $\sigma(\cdot)$ in QNNs of our consideration.

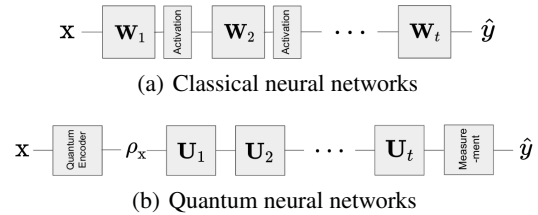


Figure 1. An illustration of layer-structured classical and quantum neural networks.

Mathematical formulation of quantum states. A general quantum state with dimension d can be represented by a *density operator* that is a positive semidefinite (PSD) Hermitian matrix $\rho \in \mathbb{C}^{d \times d}$ with $\text{tr}(\rho) = 1$. A quantum state ρ is *pure* if $\rho = \mathbf{v}\mathbf{v}^\dagger$ for a ℓ_2 unit vector \mathbf{v} . A two-dimensional quantum state $\rho \in \mathbb{C}^{2 \times 2}$ is usually referred as a *qubit*, the

quantum generalization of the classical binary bit. The state of n qubits lies in $\otimes_{i=1}^n \mathbb{C}^{2 \times 2}$ following the tensor product of spaces for single qubits, and is a linear operator on a Hilbert space with dimension $d = 2^n$, i.e., scales *exponentially* with the number of qubits n .

Parameterization of quantum transformations. Instead of directly parameterized matrices W_i , QNNs typically consist of *classically parameterized* quantum gates. A general form of these gates is $\exp(-i\theta\mathbf{H})$, where θ is the parameter, \mathbf{H} the Hamiltonian (i.e., a Hermitian matrix), and the exponential is a *matrix* exponential. For example, a commonly used gate set, called the Pauli rotation gate (e.g., Farhi et al. (2020); Li et al. (2017); Ostaszewski et al. (2019)), can be expressed as $\exp(-i\theta\mathbf{P}_c)$ (on c -th qubit) or $\exp(-i\theta\mathbf{P}_c \otimes \mathbf{P}_{c'})$ (on c -th and c' -th qubits), where \mathbf{P}_c refers to Pauli \mathbf{X} , \mathbf{Y} , \mathbf{Z} matrices.¹ We can also group gates in QNNs with respect to the layer structure in Figure 1 by putting gates that can be executed in parallel in the same layer. For example, let $\mathbf{V}_{i,j}(\theta_{i,j}) = \exp(-i\theta_{i,j}\mathbf{H}_{i,j})$ be the j th gate in the i th layer. Then $\mathbf{U}_i(\boldsymbol{\theta}) = \prod_j \mathbf{V}_{i,j}(\theta_{i,j})$ and

$$\mathbf{U}(\boldsymbol{\theta}) = \mathbf{U}_t(\boldsymbol{\theta})\mathbf{U}_{t-1}(\boldsymbol{\theta}) \cdots \mathbf{U}_1(\boldsymbol{\theta}), \quad (3)$$

where $\mathbf{U}(\boldsymbol{\theta})$ refers to the unitary transformation of the entire QNN with parameters $\boldsymbol{\theta}$. For technical convenience and to highlight the dependence on the number of parameters p , we can also write

$$\mathbf{U}(\boldsymbol{\theta}) = \mathbf{V}_p(\theta_p)\mathbf{V}_{p-1}(\theta_{p-1}) \cdots \mathbf{V}_1(\theta_1), \quad (4)$$

with $\mathbf{V}_l(\theta_l) = e^{-i\theta_l\mathbf{H}_l}$ for Hamiltonian \mathbf{H}_l and $l \in [p]$.

Quantum measurements and observables. Quantum *observables*, mathematically formulated as Hermitian matrices $\mathbf{M} \in \mathbb{C}^{d \times d}$, are used in quantum mechanics to encode the information of the classical random outcomes generated by quantum *measurements* on quantum states. The expected outcome \hat{y} of observable M on the output state $\mathbf{U}(\boldsymbol{\theta})\rho\mathbf{U}^\dagger(\boldsymbol{\theta})$ of any QNN $\mathbf{U}(\boldsymbol{\theta})$ is given by

$$\hat{y} = f(\boldsymbol{\rho}, \boldsymbol{\theta}) = \text{tr}(\mathbf{U}(\boldsymbol{\theta})\rho\mathbf{U}^\dagger(\boldsymbol{\theta})\mathbf{M})$$

or $\text{tr}(\mathbf{v}^\dagger\mathbf{U}^\dagger(\boldsymbol{\theta})\mathbf{M}\mathbf{U}(\boldsymbol{\theta})\mathbf{v})$ when $\boldsymbol{\rho} = \mathbf{v}\mathbf{v}^\dagger$.

A more complete introduction to quantum mechanics and QNNs can be found in S.M. Sect. A.

Given a quantum training set $\mathcal{S} = \{(\boldsymbol{\rho}_i, y_i)\}_{i=1}^m$ and a QNN with output $\hat{y} = f(\boldsymbol{\rho}, \boldsymbol{\theta})$, the empirical risk minimization with square loss optimizes the following loss function:

$$\mathbf{1}\mathbf{X} = \begin{bmatrix} 0 & 1 \\ 1 & 0 \end{bmatrix}, \mathbf{Y} = \begin{bmatrix} 0 & -i \\ i & 0 \end{bmatrix}, \mathbf{Z} = \begin{bmatrix} 1 & 0 \\ 0 & -1 \end{bmatrix}. \text{ For Pauli matrix } \mathbf{Z}, \exp(-i\theta\mathbf{Z}) = \begin{bmatrix} e^{-i\theta} & 0 \\ 0 & e^{i\theta} \end{bmatrix}.$$

$$L(\boldsymbol{\theta}; \mathcal{S}) = \frac{1}{m} \sum_{i=1}^m \left(\text{tr}(\mathbf{U}(\boldsymbol{\theta})\boldsymbol{\rho}_i\mathbf{U}^\dagger(\boldsymbol{\theta})\mathbf{M}) - y_i \right)^2. \quad (5)$$

When quantum encoding states are pure, namely $\boldsymbol{\rho}_i = \mathbf{v}_i\mathbf{v}_i^\dagger$ for $i \in [m]$, the loss function becomes

$$L(\boldsymbol{\theta}; \mathcal{S}) = \frac{1}{m} \sum_{j=1}^m \left(\mathbf{v}_j^\dagger\mathbf{U}^\dagger(\boldsymbol{\theta})\mathbf{M}\mathbf{U}(\boldsymbol{\theta})\mathbf{v}_j - y_j \right)^2 \quad (6)$$

which resembles Eqn.(2) from one-hidden layer neural networks with quadratic activation except for unitary transformations. It is known in (Du & Lee, 2018) that such neural networks do not possess spurious local minima almost certainly, whereas we establish a completely different behavior for QNNs.

Characterization of the landscape. For a differentiable function F defined on an unconstrained domain, $\boldsymbol{\theta}^*$ is a *critical* point if and only if the gradient vanishes at the point: $\nabla F(\boldsymbol{\theta}^*) = \mathbf{0}$. $\boldsymbol{\theta}$ is a local minimum if and only if there is an open set U containing $\boldsymbol{\theta}^*$ such that $F(\boldsymbol{\theta}^*) \leq F(\boldsymbol{\theta})$ for all $\boldsymbol{\theta} \in U$. A local minimum is global if the minimum value of F is attained at $\boldsymbol{\theta}^*$. For twice-differentiable function over an unconstrained domain, $\boldsymbol{\theta}^*$ is a local minimum if the Hessian is positive definite at $\boldsymbol{\theta}^*$ (sufficient condition) and only if $\boldsymbol{\theta}^*$ is a critical point (necessary condition).

Note further that the form of quantum gates $\exp(-i\theta\mathbf{H})$ will be *periodic* in θ for \mathbf{H} with rational eigenvalues, which is typically true for commonly used \mathbf{H} (e.g., Pauli matrices). It hence suffices to study the number of (spurious) local minima of the loss function within one period.

3. Exponentially Many Spurious Local Minima for Under-parameterized QNNs

In this section, we present our main result on the constructions of datasets for p -parameter quantum neural network instances with $\Omega(2^p)$ spurious local minima. We consider QNNs defined in Eqn. (4), with parameterized gates $\mathbf{V}_l(\theta_l)$ generated by \mathbf{H}_l with eigenvalues ± 1 . This is the case for single-qubit parameterized gates and two-qubit gates generated by Kronecker products of Pauli matrices.

Shifting \mathbf{H}_l by $\lambda\mathbf{I}$ for any $\lambda \in \mathbb{R}$ introduces a global phase factor to the output state and does not change the output $f(\boldsymbol{\rho}, \boldsymbol{\theta})$. Also, shifting the observable \mathbf{M} by $\lambda\mathbf{I}$ is equivalent to shifting the labels in the dataset by $-\lambda$. Without loss of generality, we assume $\text{tr}(\mathbf{H}_l) = 0$ and $\text{tr}(\mathbf{M}) = 0$.

We start by characterizing the output $f(\boldsymbol{\rho}, \boldsymbol{\theta})$. For any $l \in$

[p], define linear maps $\Phi_l^{(0)}(\cdot)$, $\Phi_l^{(1)}(\cdot)$ and $\Phi_l^{(2)}(\cdot)$ such that

$$\Phi_l^{(0)}(\mathbf{A}) = \frac{1}{2}(\mathbf{A} + \mathbf{H}_l \mathbf{A} \mathbf{H}_l) \quad (7)$$

$$\Phi_l^{(1)}(\mathbf{A}) = \frac{1}{2}(\mathbf{A} - \mathbf{H}_l \mathbf{A} \mathbf{H}_l) \quad (8)$$

$$\Phi_l^{(2)}(\mathbf{A}) = \frac{i}{2}[\mathbf{H}_l, \mathbf{A}] \quad (9)$$

Here $[\cdot, \cdot]$ is the commutator of two matrices. For any Hermitian \mathbf{A} , $\Phi_l^{(0)}(\mathbf{A})$ commutes with \mathbf{H}_l , and the output of $\Phi_l^{(1)}$ and $\Phi_l^{(2)}$ anti-commute with \mathbf{H}_l . For any vector $\xi \in \{0, 1, 2\}^p$, define:

$$\Phi_\xi(\mathbf{A}) = \Phi_1^{(\xi_1)} \circ \Phi_2^{(\xi_2)} \circ \dots \circ \Phi_p^{(\xi_p)}(\mathbf{A}) \quad (10)$$

with \circ denoting the composition of mappings.

The observable in Heisenberg picture $\mathbf{M}(\theta) := \mathbf{U}^\dagger(\theta) \mathbf{M} \mathbf{U}(\theta)$ can be expanded as:

$$\sum_{\xi \in \{0,1,2\}^p} \Phi_\xi(\mathbf{M}) \prod_{l:\xi_l=1} \cos 2\theta_l \prod_{l':\xi_{l'}=2} \sin 2\theta_{l'} \quad (11)$$

The QNN output $f(\rho, \theta) = \text{tr}(\rho \mathbf{M}(\theta))$ can be expressed as the following trigonometric polynomial:

$$\sum_{\xi \in \{0,1,2\}^p} \text{tr}(\rho \Phi_\xi(\mathbf{M})) \prod_{l:\xi_l=1} \cos 2\theta_l \prod_{l':\xi_{l'}=2} \sin 2\theta_{l'} \quad (12)$$

As shown in S.M. Sect. B, the loss function remains invariant under the joint transformation $\theta_l \mapsto \theta_l + \frac{\pi}{2}$ and

$$\Phi_l^{(0)}(\cdot) \mapsto \mathbf{H}_l \Phi_l^{(0)}(\cdot) \mathbf{H}_l = \Phi_l^{(0)}(\cdot) \quad (13)$$

$$\Phi_l^{(1)}(\cdot) \mapsto \mathbf{H}_l \Phi_l^{(1)}(\cdot) \mathbf{H}_l = -\Phi_l^{(1)}(\cdot) \quad (14)$$

$$\Phi_l^{(2)}(\cdot) \mapsto \mathbf{H}_l \Phi_l^{(2)}(\cdot) \mathbf{H}_l = -\Phi_l^{(2)}(\cdot) \quad (15)$$

Under the transformation $\theta_l \mapsto \theta_l + \frac{\pi}{2}$, terms in Eqn. (12) associated with $\xi : \xi_l = 0$ are invariant, while terms associated with $\xi : \xi_l = 1, 2$ flip signs.

From an alternative perspective, $L(\theta; \mathcal{S})$ contains *oscillating wave* components proportional to $\cos 4\theta_l$, $\sin 4\theta_l$, $\cos 2\theta_l$ and $\sin 2\theta_l$, hence periodic with π on each coordinate. However, due the existence of lower frequency, the periodicity with $\frac{\pi}{2}$ does not always hold for all datasets. Our construction utilizes the presence and absence of this $\frac{\pi}{2}$ -translational symmetry.

We will focus on a general class of QNN, which we call *QNN with linear independence*:

Definition 1 (QNN with linear independence). A QNN is said to be with linear independence, if the associated set of $3^p - 1$ operators $\{\Phi_\xi(\mathbf{M})\}_{\xi \in \{0,1,2\}^p, \xi \neq \mathbf{0}}$ forms a linearly independent set.

Note that for the linear independence condition to hold, the dimension of the QNN $d \geq 3^{p/2}$. Namely, it is a under-parameterized case, which differentiates us from the over-parameterized ones (Rabitz et al., 2004; Russell et al., 2016; Kiani et al., 2020). Our main result states:

Theorem 2 (Construction: exponentially many local minima). *Consider QNNs composed of unitaries generated by two-level Hamiltonians, parameterized by $\theta \in \mathbb{R}^p$. If the QNN is with linear independence, a dataset \mathcal{S} can be constructed to induce a loss function $L(\theta; \mathcal{S})$ with 2^p local minima within each period, and $2^p - 1$ of these minima are spurious with positive suboptimality gap.*

Proof of Theorem 2. The dataset we construct is composed of two parts \mathcal{S}_0 and \mathcal{S}_1 . The first component of the loss function $L(\theta; \mathcal{S}_0)$ is constructed with 2^p local minima using the $\frac{\pi}{2}$ -translational symmetry:

Lemma 3 (Creating symmetry). *For QNNs with linear independence as mentioned in Theorem 2, a dataset \mathcal{S}_0 can be constructed to induce a loss function $L(\theta; \mathcal{S}_0)$ that (1) has a local minimum at some θ^* , and (2) is invariant under translation $\theta_l \mapsto \theta_l + \frac{\pi}{2}$ for all $l \in [p]$.*

Due to the translational invariance, for any $\zeta \in \{0, 1\}^p$, $\theta^* + \frac{\pi}{2} \zeta$ is a local minimum for $L(\theta; \mathcal{S}_0)$, forming a total of 2^p local minima. A second dataset \mathcal{S}_1 is introduced to break this symmetry, creating spurious local minima:

Lemma 4 (Breaking symmetry). *Consider the QNN, dataset \mathcal{S}_0 and local minimum θ^* defined in Lemma 3. Let Θ denote the set of 2^p local minima due to the translational invariance. There exists a dataset \mathcal{S}_1 such that*

$$\inf_{\theta \in \mathcal{N}(\theta^*)} L(\theta; \mathcal{S}_0) + L(\theta; \mathcal{S}_1) < \inf_{\theta \in \mathcal{N}(\theta')} L(\theta; \mathcal{S}_0) + L(\theta; \mathcal{S}_1) \quad (16)$$

for all $\theta' \in \Theta \setminus \{\theta^*\}$, and that

$$L(\theta; \mathcal{S}_0) + L(\theta; \mathcal{S}_1) > L(\theta'; \mathcal{S}_0) + L(\theta'; \mathcal{S}_1) \quad (17)$$

for all $\theta' \in \Theta$ and all $\theta \in \partial \mathcal{N}(\theta')$. Here $\mathcal{N}(\cdot)$ denote a bounded and closed neighbourhood, such that $\mathcal{N}(\theta) \cap \mathcal{N}(\theta') = \emptyset$ for any $\theta, \theta' \in \Theta$. And let $\partial \mathcal{N}$ denote its boundary.

Eqn. (17) in Lemma 4 ensures the existence of a local minimum within $\mathcal{N}(\theta)$ for each $\theta \in \Theta$, and Eqn. (16) promises that only the local minimum within $\mathcal{N}(\theta^*)$ achieves the global optimal value. Combining \mathcal{S}_0 and \mathcal{S}_1 finishes the proof for Theorem 2. \square

We give proof sketches for Lemma 3 and 4. The full proofs are postponed to S.M. Sect. B.

Proof sketch for Lemma 3. It suffices to construct a dataset $\mathcal{S}_0 = \{(\rho_k, y_k)\}_{k=1}^{m_0}$, such that (1) for all $k \in [p]$, $f_k(\theta) := \langle \rho_k, \mathbf{M}(\theta) \rangle - y_k$ is either symmetric or anti-symmetric under $\theta_l \mapsto \theta_l + \frac{\pi}{2}$ for all $l \in [p]$, and (2) the intersection Θ of the set of roots Θ_k of $f_k(\theta) = 0$ is non-empty and contains at least one isolated point θ^* . For such \mathcal{S}_0 , θ^* is an isolated root of the non-negative loss function $L(\theta; \mathcal{S}_0) = \sum_{k=1}^{m_0} f_k(\theta)^2$.

The existence of such dataset \mathcal{S}_0 follows from the linear independence of operators for the QNN. As a result, for any $k \in [m_0]$, the solution to the following linear system for Hermitian $\mathbf{D}_k \in \mathbb{C}^{d \times d}$ is non-empty:

$$\begin{cases} \text{tr}(\mathbf{D}_k \cdot \mathbf{I}) = 0, \\ \text{tr}(\mathbf{D}_k \cdot \Phi_{\xi}(\mathbf{M})) = \hat{f}_{\xi,k}, \quad \forall \xi \neq \mathbf{0}. \end{cases} \quad (18)$$

Here $\hat{f}_{\xi,k}$ is the coefficient corresponding to the term $\prod_{l:\xi_l=1} \cos 2\theta_l \prod_{l':\xi_{l'}=2} \sin 2\theta_{l'}$ in $f_k(\theta)$. Given the solution $\{\mathbf{D}_k\}_{k=1}^{m_0}$, \mathcal{S}_0 can be constructed by setting $\rho_k := \frac{1}{d}\mathbf{I} + \kappa\mathbf{D}_k$ for a proper scaling factor κ and let $y_k = \text{tr}(\rho_k \Phi_{\mathbf{0}}(\mathbf{M}))$. \square

Proof sketch for Lemma 4. Rewrite the loss function as

$$\begin{aligned} L(\theta; \mathcal{S}_1) &= -\frac{2}{m_1} \sum_{k=1}^{m_1} y_k \text{tr}(\rho_k \mathbf{M}(\theta)) \\ &+ \frac{1}{m_1} \sum_{k=1}^{m_1} \text{tr}(\rho_k \mathbf{M}(\theta))^2 + \frac{1}{m_1} \sum_{k=1}^{m_1} y_k^2 \end{aligned} \quad (19)$$

As will be made clear in S.M. Sect. B, our key observation is that, under a joint scaling of y_k and ρ_k , the second term can be arbitrarily suppressed while the first term remains the same. Therefore it suffices to study the first term $L'(\theta; \mathcal{S}_1) := -\frac{2}{m_1} \sum_{k=1}^{m_1} y_k \text{tr}(\rho_k \mathbf{M}(\theta))$. The linear independence allows us to solve a linear system to construct \mathcal{S}_1 that satisfies the requirements in Lemma 4. \square

Remarks. The statements above involve unitaries generated by two-level Hamiltonians only. For more general local quantum gates, $\{\mathbf{H}_l\}_{l=1}^p$ are allowed to have more than two distinct eigenvalues. We are especially interested in Hamiltonians with eigenvalues $\{E_1, \dots, E_d\} \subset \mathbb{Z}$, as arbitrary Hamiltonians with rational spectrum can be converted to ones with integral spectrum with proper shifting and scaling. Theorem 2 can be generalized for \mathbf{H}_l 's with largest eigen-gap $\max_{c,c' \in [d]} |E_c - E_{c'}|$ bounded by Δ , with the number of spurious local minima being $\Omega(\Delta^p)$. This observation further supports the intuition of interference as the source of local minima.

1-layer QNN. A simple example of QNNs with linear independence is a one-layer circuit with local \mathbf{H}_l acting on the l -th qubit, and a product operator \mathbf{M} as the observable:

Proposition 5 (One-layer QNNs with product observables). *Consider the family of QNNs composed of unitaries generated by two-level Hamiltonians, parameterized by $\theta \in \mathbb{R}^p$. For all $l \in [p]$, let \mathbf{H}_l be a local Hamiltonian on the l -qubit, taking the form $\mathbf{I} \otimes \dots \otimes \mathbf{h}_l \otimes \dots \otimes \mathbf{I}$ for some Hermitian \mathbf{h}_l at the l -th position, and $\mathbf{M} = \mathbf{m}_1 \otimes \dots \otimes \mathbf{m}_p$ such that $\mathbf{m}_l + \mathbf{h}_l \mathbf{m}_l \mathbf{h}_l$ and $\mathbf{m}_l - \mathbf{h}_l \mathbf{m}_l \mathbf{h}_l$ are non-zero for any l . There exists a dataset that induces a loss function with $2^p - 1$ spurious local minima.*

This follows from the fact that $\text{tr}(\Phi_{\xi}(\mathbf{M})\Phi_{\xi'}(\mathbf{M})) = 0$ if and only if $\xi \neq \xi'$. In S.M. Sect. B, we provide proof for Proposition 5 and several concrete example QNNs to demonstrate that our construction can have local minima at arbitrary θ , and does not allow trivial solutions such as coordinate-wise greedy optimization.

4. Typical QNNs are with Linear Independence

In Section 3, we provided a general condition (Definition 1) for QNNs to have exponentially many bad local minima for some datasets. In this section, we show that this condition is met for typical under-parameterized QNNs. To see this, we consider the following measure over instances of QNNs: Let \mathbf{H} be a d -dimensional Hermitian such that $\text{tr}(\mathbf{H}) = 0$ and $\mathbf{H}^2 = \mathbf{I}$. A random circuit $\mathbf{U}(\theta)$ is specified as

$$\mathbf{U}(\theta) = e^{-i\theta_p \mathbf{W}_p \mathbf{H} \mathbf{W}_p^\dagger} \dots e^{-i\theta_1 \mathbf{W}_1 \mathbf{H} \mathbf{W}_1^\dagger} \quad (21)$$

with $\{\mathbf{W}_l\}_{l=1}^p$ independently sampled with respect to the Haar measure on the d -dimensional unitary group $U(d)$.

Up to a unitary transformation, this random model is equivalent to a circuit with p interleaving parameterized gate $\{e^{-i\theta_l \mathbf{H}}\}_{l=1}^p$ and unitary $\{\tilde{\mathbf{W}}_l\}_{l=1}^p$ randomly sampled with respect to the Haar measure:

$$\mathbf{U}(\theta) = \tilde{\mathbf{W}}_p e^{-i\theta_p \mathbf{H}} \tilde{\mathbf{W}}_{p-1} \dots \tilde{\mathbf{W}}_1 e^{-i\theta_1 \mathbf{H}} \quad (22)$$

The equivalence is due to the left (or right) invariance of the Haar measure. This interleaving nature of fixed and parameterized gates are shared by existing designs of QNNs, and any p -parameter QNN generated by two-level Hamiltonians can be expressed in Eqn. (22). Moreover, applying polynomially many random 2-qubit gates on random pairs of qubits generates a distribution over gates that approximates the Haar measure up to the 4-th moments (Brandao et al., 2016), which is what we require in this section.

The Gram matrix for the set $\{\Phi_{\xi}(\mathbf{M})\}_{\xi \in \{0,1,2\}^p, \xi \neq \mathbf{0}}$ is defined such that the element corresponding to the pair (ξ, ξ') is $\text{tr}(\Phi_{\xi}(\mathbf{M})\Phi_{\xi'}(\mathbf{M}))$. The Gram matrix is always positive semidefinite, and a positive definite Gram matrix implies the linear independence of the set.

Using the integral formula with respect to Haar measure on unitary groups (Puchała & Miszczak, 2011), we can

estimate the expectations and variances of the diagonal and off-diagonal terms, and upper bound the probability of the event:

$$\exists \xi : \text{tr}(\Phi_\xi(\mathbf{M})^2) \leq \sum_{\xi' \neq \xi} |\text{tr}(\Phi_\xi(\mathbf{M})\Phi_{\xi'}(\mathbf{M}))| \quad (23)$$

Applying the Gershgorin circle theorem (Golub & Van Loan, 1996), we can lower bound the probability for a random QNN to have linear independent terms:

Theorem 6 (Typical under-parameterized QNNs are with linear independence). *Consider a random p -parameter d -dimensional QNN with two-level Hamiltonians sampled from the model specified in Eqn. (21). Let the observable \mathbf{M} be an arbitrary non-zero trace-0 Hermitian. Such QNN is with linear independence with probability $\geq 1 - O(d^{-1})$ for fixed p , and with probability $\geq 1 - O(e^{-p})$ for dimension $d : \log(d) = \Theta(p)$.*

Please refer to S.M. Sect. C for the full proof.

5. Upper Bound on the Number of Local Minima

Our construction above possesses 2^p local minima for p parameters, whereas the classical work of Auer et al. (1996) demonstrates a construction for a single neuron with $[m/p]^p$ local minima for m training samples. Note that the latter could grow unboundedly with m . In this section, we show, however, this classical unbounded growth of local minima does not hold for QNNs. In fact, we could establish an almost matching upper bound for 2^p . All the formal proofs are deferred to S.M. Sect. D.

To that end, let us examine the *Fourier* expansion of the loss function $L(\theta, \mathcal{S})$ (Eqn. (5)). Let T_l be the period of $L(\theta; \mathcal{S})$ corresponding to θ_l , and $\hat{L}(\mathbf{k})$ the Fourier coefficient for $\mathbf{k} = (k_1, \dots, k_p)^T \in \mathbb{Z}^p$. We have

$$L(\theta; \mathcal{S}) = \sum_{\mathbf{k} \in K} \hat{L}(\mathbf{k}) \prod_{l=1}^p \left(\cos \frac{k_l \theta_l}{T_l} + i \sin \frac{k_l \theta_l}{T_l} \right) \quad (24)$$

where $K \subseteq \mathbb{Z}^p$ is the support of the Fourier coefficients.

One critical observation is that, for arbitrary choice of two-level $\{\mathbf{H}_l\}_{l=1}^p$, observable \mathbf{M} and training set \mathcal{S} , the support K of the Fourier spectrum is bounded in ℓ_1 -norm: $\max_{\mathbf{k} \in K} \sum_{l=1}^p |k_l| \leq 2p$, indicating that the Fourier degree of $L(\theta; \mathcal{S})$ is upper bounded by $2p$ (See S.M. Sect. D.1).

By definition, a local minimum must be a critical point, hence it suffices to bound the number of critical points for functions with Fourier spectrum supported on a ℓ_1 -bounded

set. Define $G_l(\theta)$ as $\frac{\partial}{\partial \theta_l} L(\theta; \mathcal{S})$:

$$G_l(\theta) = \sum_{\mathbf{k} \in K} k_l \hat{L}(\mathbf{k}) \left(-\sin \frac{k_l \theta_l}{T_l} + i \cos \frac{k_l \theta_l}{T_l} \right) \quad (25)$$

$$\cdot \prod_{l' \neq l} \left(\cos \frac{k_{l'} \theta_{l'}}{T_{l'}} + i \sin \frac{k_{l'} \theta_{l'}}{T_{l'}} \right) \quad (26)$$

Notice that the Fourier spectrum of G_l is supported on the same set K . A critical point of $L(\theta; \mathcal{S})$ must satisfy that for all $l \in [p]$, $G_l(\theta) = 0$. By basic trigonometry, $\cos k\theta$ can be expressed as a degree- k polynomial of $\cos \theta$ and $\sin k\theta$ as a degree- $(k-1)$ polynomial of $\cos \theta$ multiplied by $\sin \theta$. Consider the change of variable

$$c_l = \cos(\theta_l/T_l), \quad s_l = \sin(\theta_l/T_l), \quad \forall l \in [p]. \quad (27)$$

Let $g_l(c_1, s_1, \dots, c_p, s_p)$ be the multivariate polynomial constraints corresponding to $G_l(\theta)$ after the change of variable. For each g_l , the sum of degrees of $c_{l'}$ and $s_{l'}$ is bounded by $\max_{\mathbf{k} \in K} |k_{l'}|$, and the degree $\deg(g_l)$ of g_l is bounded by $\max_{\mathbf{k} \in K} \sum_{l=1}^p |k_l| \leq 2p$. The change of variable is one-to-one from $\theta_l \in [0, T_l)$ to a pair of $(c_l, s_l) \in \mathbb{R}^2$ under the constraint $c_l^2 + s_l^2 = 1$. Therefore, it suffices to count the number of roots of the polynomial system with $2p$ parameters and $2p$ constraints:

$$g_l(c_1, s_1, \dots, c_p, s_p) = 0, \quad c_l^2 + s_l^2 - 1 = 0 \quad (28)$$

for all $l \in [p]$. Notice that for a general polynomial system, the number of critical points can be unbounded. For example, consider a system composed of constant polynomials, every point in the domain is a critical point. This corresponds to the constant loss function, where the gradients vanish everywhere with positive semidefinite Hessians. For this reason, we will focus on the non-degenerated case with finitely many local minima. Under the premise of non-degeneracy, by Bézout's Theorem (e.g. Section 3.3 in Cox et al. (2006)), the number of roots can be bounded by the product of the degree of polynomial constraints $2^p \deg(g_1) \deg(g_2) \dots \deg(g_p) \leq (4p)^p$. A formal statement of the above derivation is as follows:

Theorem 7 (Upper bound: the number of local minima). *Consider non-degenerated QNNs composed of unitaries generated by two-level Hamiltonians $\{\mathbf{H}_l\}_{l=1}^p$ with p parameters. For training set \mathcal{S} , within each period, the loss function $L(\theta; \mathcal{S})$ possesses at most $(4p)^p$ local minima.*

We also prove a similar result for the more general case where the generators are Hamiltonians with integral spectrum: let Δ be the largest eigen-gap for each of the Hamiltonians, the number of local minima within each period is upper bounded by $O((\Delta p)^p)$. Please refer to S.M. Sect. D for details.

6. Experiments

We investigate the practical performance of the common optimizers on our construction in this section. It is well-known in the classical literature that the existence of spurious local minima does not necessarily cause difficulties in optimization (e.g., Ge & Ma (2017)). We show, however, our constructions can indeed be hard instances for training in practice.

To that end, we evaluate a specific construction from Proposition 5 in Section 3 by using the standard optimizers with randomly initialized parameters uniformly sampled from the domain², and visualize the distribution of function values at convergence. For p -parameter instances, our construction involves p -qubits. We choose $\mathbf{h}_1 = \dots = \mathbf{h}_p = \mathbf{Z}$ and $\mathbf{m}_1 = \dots = \mathbf{m}_p = \mathbf{Y} + \mathbf{I}$. The specific form of the instance and all the training details are provided in S.M. Sect. E.

Implementation The experiments are run on Intel Core i7-7700HQ Processor (2.80GHz) with 16G memory. We classically simulate the training with Pytorch (Paszke et al., 2019), using the analytical form of the objective function for the purpose of efficiency.

Optimizers The QNN instances are trained with three popular optimizers in classical optimization or machine learning: Adam(Kingma & Ba, 2015), RMSProp(Bengio, 2015), and L-BFGS(Liu & Nocedal, 1989). The first two methods (Kingma & Ba, 2015; Bengio, 2015) are variants of vanilla gradient descent with adaptive learning rate. and are widely used for training large-scale deep neural networks as well as for the quantum counterparts (Killoran et al., 2019; Mari et al., 2020; Lloyd et al., 2020; Ostaszewski et al., 2019; Sweke et al., 2020). The last method (Liu & Nocedal, 1989) is an efficient implementation of the approximate Newton method that utilizes the second-order information (i.e. the Hessian). For all instances and optimizers, we use the exact gradient induced by the dataset without stochasticity from the mini-batched gradient descent.

It turns out, for all the examined instances and all three optimizers, under random initialization, the optimizations converge to local minima with non-negligible suboptimality (i.e., different from the global one by a non-negligible amount) with high probability. In Figure 2, we train the 4-parameter construction with RMSProp and repeat for 100 times. Let θ_i and θ_f denote the parameters at initialization and at convergence. The function values at initialization $L(\theta_i; \mathcal{S})$ are supported on a continuous spectrum as shown in gray. After training and converging with RMSProp, the function values $L(\theta_f; \mathcal{S})$ fall into discretized values as shown in orange. The smallest training loss attainable in our

²For p -parameter instances, we uniformly sample the initial parameters from $[0, 2\pi)^p$.

construction is 0, therefore only the leftmost bar (to the left of the dotted **black** vertical line) corresponds to the global minimum. Namely, the success probability of converging to the global minimum is very small. A similar phenomenon persists for instances with more parameters and with different optimizers in Figure 3. As the number of bad local minima grows exponentially in our construction, the success probability should also in theory decay exponentially. This is empirically confirmed in Figure 4, where we illustrate the precise empirical success probability for all these tests. Moreover, as shown in S.M. Sect. E.3, the tendency of exponential decay remains unchanged in the presence of label noises, indicating the robustness of our constructions.

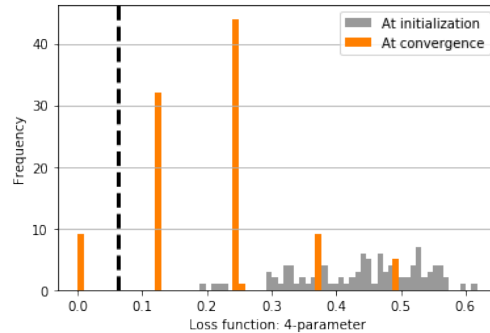


Figure 2. Loss functions at random initialization and at convergence for 4-parameter instances trained with RMSProp, repeated for 100 times. The function values are supported on a continuous spectrum at initialization as plotted in gray and converge to discretized values as plotted in orange.

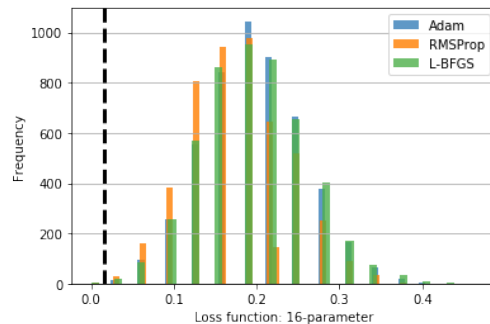


Figure 3. Distributions of loss functions at convergence for instances with 16 parameters trained with Adam, RMSProp and L-BFGS, repeated 5000 times with uniformly random initialization. All methods fail to converge to the global minimum 0.0 with high probability.

Beyond the constructed datasets To demonstrate the generality of our results, we repeat the experiments for datasets with more practical significance: for p -parameter instances, we choose the input state to be a p -qubit encoding of $\mathbf{x} \in [0, 2\pi)^{2p}$ via \mathbf{X} - and \mathbf{Y} -rotations on each of

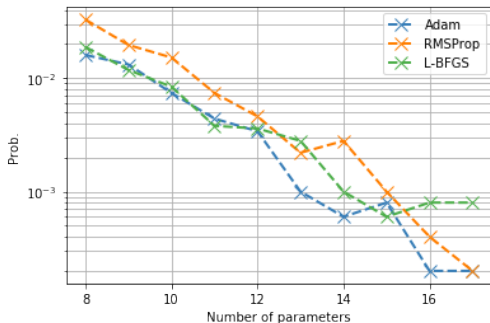


Figure 4. The decay of success rate for finding the global minimum under random initialization with Adam, RMSProp, L-BFGS. For each data point, we repeat the experiments for 5000 times.

the qubits. The associated label is either 1 or 0, depending on the sign of $\mathbf{w}^T \mathbf{x}$, with \mathbf{w} being the normal vector of a hyperplane in \mathbb{R}^{2^p} . These datasets have the interpretation as an encoding of a linearly separable classical concept. In Figure 5, we plot the function values at convergence for an 8-parameter instance: no more than 4 of the 70 random initializations have reached the global minima. This is repeated for instances with 2, 4 and 6 qubits. While we no longer have a clear exponential dependency in the success rate, the number of local minima increases significantly as the number of parameters increases (see S.M. Sect. E.4). This observation suggests that our theory and experiments on the constructed datasets can capture the practical difficulty in training under-parameterized QNNs with gradient-based methods.

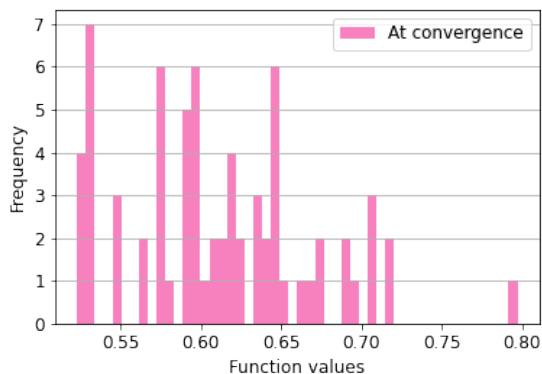


Figure 5. Function values at convergence for training an 8-parameter instance with RMSProp on the linearly-separable classical concept. No more than 4 among the 70 random initializations find the global minima, indicating the existence of many sub-optimal local minima.

7. Conclusion

In this work, we provide a characterization of the landscape for under-parameterized QNNs, by showing that in the worst-case, the number of local minima can increase exponentially with the number of parameters. Supported by numerical simulations, our result suggests when under-parameterized, QNNs may not be efficiently solved by gradient-based black-box methods.

This work leaves several open questions:

- Given the knowledge of the data distribution, can we design a QNN architecture with a benign landscape?
- We know that when sufficiently parameterized (e.g. (Russell et al., 2016)), the landscape for optimizing variational quantum ansatz can be benign. It is therefore natural to ask, fixing the system size, how does the landscape change as the number of parameters increases?
- Classically, despite the provable bad landscape of shallow neural networks (e.g. Safran & Shamir (2018)), Goel & Klivans (2019) came up with algorithms that can minimize the loss with guarantees. Can we design an algorithm (beyond gradient-based method) that can solve the optimization problem efficiently and provably?

Acknowledgements

We thank reviewers for useful comments. This work received support from the U.S. Department of Energy, Office of Science, Office of Advanced Scientific Computing Research, Accelerated Research in Quantum Computing and Quantum Algorithms Team programs, as well as the U.S. National Science Foundation grant CCF-1755800, CCF-1816695, and CCF-1942837 (CAREER).

References

- Arora, S., Du, S. S., Hu, W., Li, Z., Salakhutdinov, R., and Wang, R. On exact computation with an infinitely wide neural net. *arXiv preprint arXiv:1904.11955*, 2019.
- Arute, F., Arya, K., Babbush, R., Bacon, D., Bardin, J. C., Barends, R., Biswas, R., Boixo, S., Brandao, F. G. S. L., Buell, D. A., Burkett, B., Chen, Y., Chen, Z., Chiaro, B., Collins, R., Courtney, W., Dunsworth, A., Farhi, E., Foxen, B., Fowler, A., Gidney, C., Giustina, M., Graff, R., Guerin, K., Habegger, S., Harrigan, M. P., Hartmann, M. J., Ho, A., Hoffmann, M., Huang, T., Humble, T. S., Isakov, S. V., Jeffrey, E., Jiang, Z., Kafri, D., Kechedzhi, K., Kelly, J., Klimov, P. V., Knysh, S., Korotkov, A., Kostritsa, F., Landhuis, D., Lindmark, M., Lucero, E.,

- Lyakh, D., Mandrà, S., McClean, J. R., McEwen, M., Megrant, A., Mi, X., Michielsen, K., Mohseni, M., Mutus, J., Naaman, O., Neeley, M., Neill, C., Niu, M. Y., Ostby, E., Petukhov, A., Platt, J. C., Quintana, C., Rieffel, E. G., Roushan, P., Rubin, N. C., Sank, D., Satzinger, K. J., Smelyanskiy, V., Sung, K. J., Trevithick, M. D., Vainsencher, A., Villalonga, B., White, T., Yao, Z. J., Yeh, P., Zalcman, A., Neven, H., and Martinis, J. M. Quantum supremacy using a programmable superconducting processor. *Nature*, 574(7779):505–510, 2019.
- Arute, F., Arya, K., Babbush, R., Bacon, D., Bardin, J. C., Barends, R., Boixo, S., Broughton, M., Buckley, B. B., Buell, D. A., Burkett, B., Bushnell, N., Chen, Y., Chen, Z., Chiaro, B., Collins, R., Courtney, W., Demura, S., Dunsworth, A., Farhi, E., Fowler, A., Foxen, B., Gidney, C., Giustina, M., Graff, R., Habegger, S., Harrigan, M. P., Ho, A., Hong, S., Huang, T., Huggins, W. J., Ioffe, L., Isakov, S. V., Jeffrey, E., Jiang, Z., Jones, C., Kafri, D., Kechedzhi, K., Kelly, J., Kim, S., Klimov, P. V., Korotkov, A., Kostritsa, F., Landhuis, D., Laptev, P., Lindmark, M., Lucero, E., Martin, O., Martinis, J. M., McClean, J. R., McEwen, M., Megrant, A., Mi, X., Mohseni, M., Mruzckiewicz, W., Mutus, J., Naaman, O., Neeley, M., Neill, C., Neven, H., Niu, M. Y., O’Brien, T. E., Ostby, E., Petukhov, A., Putterman, H., Quintana, C., Roushan, P., Rubin, N. C., Sank, D., Satzinger, K. J., Smelyanskiy, V., Strain, D., Sung, K. J., Szalay, M., Takeshita, T. Y., Vainsencher, A., White, T., Wiebe, N., Yao, Z. J., Yeh, P., and Zalcman, A. Hartree-fock on a superconducting qubit quantum computer. *Science*, 369(6507):1084–1089, 2020. ISSN 0036-8075. doi: 10.1126/science.abb9811. URL <https://science.sciencemag.org/content/369/6507/1084>.
- Auer, P., Herbster, M., and Warmuth, M. K. Exponentially many local minima for single neurons. In *Advances in neural information processing systems*, pp. 316–322, 1996.
- Benedetti, M., Lloyd, E., Sack, S., and Fiorentini, M. Parameterized quantum circuits as machine learning models. *Quantum Science and Technology*, 4(4):043001, 2019.
- Bengio, Y. Rmsprop and equilibrated adaptive learning rates for nonconvex optimization. *corr abs/1502.04390*, 2015.
- Biamonte, J., Wittek, P., Pancotti, N., Rebentrost, P., Wiebe, N., and Lloyd, S. Quantum machine learning. *Nature*, 549(7671):195, 2017.
- Brandao, F. G., Harrow, A. W., and Horodecki, M. Local random quantum circuits are approximate polynomial-designs. *Communications in Mathematical Physics*, 346(2):397–434, 2016.
- Collins, B. and Śniady, P. Integration with respect to the haar measure on unitary, orthogonal and symplectic group. *Communications in Mathematical Physics*, 264(3):773–795, 2006.
- Cox, D. A., Little, J., and O’Shea, D. *Using algebraic geometry*, volume 185. Springer Science & Business Media, 2006.
- Ding, T., Li, D., and Sun, R. Sub-optimal local minima exist for almost all over-parameterized neural networks. *arXiv preprint arXiv:1911.01413*, 2019.
- Du, S. and Lee, J. On the power of over-parametrization in neural networks with quadratic activation. In *International Conference on Machine Learning*, pp. 1329–1338. PMLR, 2018.
- Du, S., Lee, J., Li, H., Wang, L., and Zhai, X. Gradient descent finds global minima of deep neural networks. In *International Conference on Machine Learning*, pp. 1675–1685. PMLR, 2019.
- Du, S. S. and Goel, S. Improved learning of one-hidden-layer convolutional neural networks with overlaps. *arXiv preprint arXiv:1805.07798*, 2018.
- Farhi, E., Goldstone, J., and Gutmann, S. A quantum approximate optimization algorithm. *arXiv preprint arXiv:1411.4028*, 2014.
- Farhi, E., Goldstone, J., Gutmann, S., and Zhou, L. The Quantum Approximate Optimization Algorithm and the Sherrington-Kirkpatrick Model at Infinite Size. *arXiv e-prints*, art. arXiv:1910.08187, October 2019.
- Farhi, E., Neven, H., et al. Classification with quantum neural networks on near term processors. *Quantum Review Letters*, 1(2 (2020)):10–37686, 2020.
- Ge, R. and Ma, T. On the optimization landscape of tensor decompositions. In *Advances in Neural Information Processing Systems*, pp. 3653–3663, 2017.
- Goel, S. and Klivans, A. R. Learning neural networks with two nonlinear layers in polynomial time. In *Conference on Learning Theory*, pp. 1470–1499. PMLR, 2019.
- Goel, S., Kanade, V., Klivans, A., and Thaler, J. Reliably learning the relu in polynomial time. In *Conference on Learning Theory*, pp. 1004–1042. PMLR, 2017.
- Golub, G. H. and Van Loan, C. F. *Matrix computations*. JHU press, 1996.
- Harrow, A. W. and Montanaro, A. Quantum computational supremacy. *Nature*, 549(7671):203–209, 2017.

- Havlíček, V., Córcoles, A. D., Temme, K., Harrow, A. W., Kandala, A., Chow, J. M., and Gambetta, J. M. Supervised learning with quantum-enhanced feature spaces. *Nature*, 567(7747):209–212, 2019.
- Horn, R. A. and Johnson, C. R. *Matrix analysis*. Cambridge university press, 2013.
- Jacot, A., Hongler, C., and Gabriel, F. Neural tangent kernel: Convergence and generalization in neural networks. In Bengio, S., Wallach, H. M., Larochelle, H., Grauman, K., Cesa-Bianchi, N., and Garnett, R. (eds.), *Advances in Neural Information Processing Systems 31: Annual Conference on Neural Information Processing Systems 2018, NeurIPS 2018, December 3-8, 2018, Montréal, Canada*, pp. 8580–8589, 2018. URL <https://proceedings.neurips.cc/paper/2018/hash/5a4belfa34e62bb8a6ec6b91d2462f5a-Abstract.html>.
- Kawaguchi, K. Deep learning without poor local minima. In *Advances in neural information processing systems*, pp. 586–594, 2016.
- Kiani, B. T., Lloyd, S., and Maity, R. Learning unitaries by gradient descent, 2020.
- Killoran, N., Bromley, T. R., Arrazola, J. M., Schuld, M., Quesada, N., and Lloyd, S. Continuous-variable quantum neural networks. *Physical Review Research*, 1(3):033063, 2019.
- Kingma, D. P. and Ba, J. Adam: A method for stochastic optimization. In Bengio, Y. and LeCun, Y. (eds.), *3rd International Conference on Learning Representations, ICLR 2015, San Diego, CA, USA, May 7-9, 2015, Conference Track Proceedings*, 2015. URL <http://arxiv.org/abs/1412.6980>.
- Li, D., Ding, T., and Sun, R. Over-parameterized deep neural networks have no strict local minima for any continuous activations. *arXiv preprint arXiv:1812.11039*, 2018.
- Li, J., Yang, X., Peng, X., and Sun, C.-P. Hybrid quantum-classical approach to quantum optimal control. *Physical review letters*, 118(15):150503, 2017.
- Liu, D. C. and Nocedal, J. On the limited memory bfgs method for large scale optimization. *Mathematical programming*, 45(1-3):503–528, 1989.
- Lloyd, S., Schuld, M., Ijaz, A., Izaac, J., and Killoran, N. Quantum embeddings for machine learning. *arXiv preprint arXiv:2001.03622*, 2020.
- Mari, A., Bromley, T. R., Izaac, J., Schuld, M., and Killoran, N. Transfer learning in hybrid classical-quantum neural networks. *Quantum*, 4:340, 2020.
- McClellan, J. R., Boixo, S., Smelyanskiy, V. N., Babbush, R., and Neven, H. Barren plateaus in quantum neural network training landscapes. *Nature communications*, 9(1):1–6, 2018.
- Mitarai, K., Negoro, M., Kitagawa, M., and Fujii, K. Quantum circuit learning. *Physical Review A*, 98(3):032309, 2018.
- Nguyen, Q. and Hein, M. The loss surface of deep and wide neural networks. In *International conference on machine learning*, pp. 2603–2612. PMLR, 2017.
- Nielsen, M. A. and Chuang, I. Quantum computation and quantum information, 2002.
- Ostaszewski, M., Grant, E., and Benedetti, M. Quantum circuit structure learning. *arXiv preprint arXiv:1905.09692*, 2019.
- Paszke, A., Gross, S., Massa, F., Lerer, A., Bradbury, J., Chanan, G., Killeen, T., Lin, Z., Gimelshein, N., Antiga, L., et al. Pytorch: An imperative style, high-performance deep learning library. In *Advances in Neural Information Processing Systems*, pp. 8024–8035, 2019.
- Peruzzo, A., McClellan, J., Shadbolt, P., Yung, M.-H., Zhou, X.-Q., Love, P. J., Aspuru-Guzik, A., and O’Brien, J. L. A variational eigenvalue solver on a photonic quantum processor. *Nature Communications*, 5:4213, 2014.
- Petz, D. A survey of certain trace inequalities. *Banach Center Publications*, 30(1):287–298, 1994.
- Petz, D. and Zemánek, J. Characterizations of the trace. *Linear Algebra and its Applications*, 111:43–52, 1988.
- Preskill, J. Quantum computing in the NISQ era and beyond. *Quantum*, 2:79, 2018. ISSN 2521-327X.
- Puchała, Z. and Miszczak, J. A. Symbolic integration with respect to the haar measure on the unitary group. *arXiv preprint arXiv:1109.4244*, 2011.
- Rabitz, H. A., Hsieh, M. M., and Rosenthal, C. M. Quantum optimally controlled transition landscapes. *Science*, 303(5666):1998–2001, 2004.
- Russell, B., Rabitz, H., and Wu, R. Quantum control landscapes are almost always trap free. *arXiv preprint arXiv:1608.06198*, 2016.
- Safran, I. and Shamir, O. Spurious local minima are common in two-layer relu neural networks. In *International Conference on Machine Learning*, pp. 4433–4441. PMLR, 2018.

- Schuld, M. and Killoran, N. Quantum machine learning in feature hilbert spaces. *Physical review letters*, 122(4): 040504, 2019.
- Soudry, D. and Carmon, Y. No bad local minima: Data independent training error guarantees for multilayer neural networks. *arXiv preprint arXiv:1605.08361*, 2016.
- Sweke, R., Wilde, F., Meyer, J. J., Schuld, M., Fahrman, P. K., Meynard-Piganeau, B., and Eisert, J. Stochastic gradient descent for hybrid quantum-classical optimization. *Quantum*, 4:314, 2020.
- Venturi, L., Bandeira, A. S., and Bruna, J. Spurious valleys in two-layer neural network optimization landscapes. *arXiv preprint arXiv:1802.06384*, 2018.
- Wang, Z., Hadfield, S., Jiang, Z., and Rieffel, E. G. Quantum approximate optimization algorithm for maxcut: A fermionic view. *Phys. Rev. A*, 97: 022304, Feb 2018. doi: 10.1103/PhysRevA.97.022304. URL <https://link.aps.org/doi/10.1103/PhysRevA.97.022304>.
- Wang, Z., Rubin, N. C., Dominy, J. M., and Rieffel, E. G. xy mixers: Analytical and numerical results for the quantum alternating operator ansatz. *Phys. Rev. A*, 101:012320, Jan 2020. doi: 10.1103/PhysRevA.101.012320. URL <https://link.aps.org/doi/10.1103/PhysRevA.101.012320>.
- Watrous, J. *The theory of quantum information*. Cambridge University Press, 2018.
- Yun, C., Sra, S., and Jadbabaie, A. Small nonlinearities in activation functions create bad local minima in neural networks. *arXiv preprint arXiv:1802.03487*, 2018.
- Zhong, H.-S., Wang, H., Deng, Y.-H., Chen, M.-C., Peng, L.-C., Luo, Y.-H., Qin, J., Wu, D., Ding, X., Hu, Y., Hu, P., Yang, X.-Y., Zhang, W.-J., Li, H., Li, Y., Jiang, X., Gan, L., Yang, G., You, L., Wang, Z., Li, L., Liu, N.-L., Lu, C.-Y., and Pan, J.-W. Quantum computational advantage using photons. *Science*, 370(6523):1460–1463, 2020. ISSN 0036-8075. doi: 10.1126/science.abe8770. URL <https://science.sciencemag.org/content/370/6523/1460>.
- Zhong, K., Song, Z., Jain, P., Bartlett, P. L., and Dhillon, I. S. Recovery guarantees for one-hidden-layer neural networks. In *International conference on machine learning*, pp. 4140–4149. PMLR, 2017.

A. Preliminaries

In this section we introduce necessary backgrounds on quantum information and linear algebra. For further readings, we refer the readers to the books by Nielsen and Chuang (Nielsen & Chuang, 2002) and by Watrous (Watrous, 2018).

A.1. Linear Algebra

Basic notions. We use $\mathbf{I}_{d \times d}$ to denote the identity matrix in $\mathbb{C}^{d \times d}$. The subscripts are omitted when there is no ambiguity on the dimension. Let \dagger denote the conjugate transpose of complex matrices. A matrix $\mathbf{U} \in \mathbb{C}^{d \times d}$ is said to be a unitary if $\mathbf{U}\mathbf{U}^\dagger = \mathbf{I}_{d \times d}$. A matrix is said to be Hermitian if its conjugate transpose is itself: $\mathbf{A} = \mathbf{A}^\dagger$. Let $[\cdot, \cdot]$ denote the commutator of two matrices, such that $[\mathbf{A}, \mathbf{B}] := \mathbf{A}\mathbf{B} - \mathbf{B}\mathbf{A}$.

Inner product and adjoints. The inner product between two Hermitians \mathbf{A} and \mathbf{B} is defined as:

$$\langle \mathbf{A}, \mathbf{B} \rangle := \text{tr}(\mathbf{A}\mathbf{B}) \quad (\text{A.1})$$

For a linear map $\Phi(\cdot)$, the adjoint of the linear map $\Phi^*(\cdot)$ is defined such that

$$\langle \mathbf{A}, \Phi(\mathbf{B}) \rangle = \langle \Phi^*(\mathbf{A}), \mathbf{B} \rangle \quad (\text{A.2})$$

The Frobenius norm of a Hermitian \mathbf{A} is defined as:

$$\|\mathbf{A}\|_F := \sqrt{\langle \mathbf{A}, \mathbf{A} \rangle} \quad (\text{A.3})$$

Exponent of matrices. The exponent of a Hermitian \mathbf{A} is defined using Taylor expansion

$$\exp(\mathbf{A}) := \sum_{k=0}^{\infty} \frac{\mathbf{A}^k}{k!}, \quad (\text{A.4})$$

Let $\{E_j\}_{j=1}^d$ and $\{\mathbf{u}_j\}_{j=1}^d$ be the eigenvalues and eigenvectors of \mathbf{A} , We have

$$\begin{aligned} \exp(\mathbf{A}) &:= \sum_{k=0}^{\infty} \frac{\mathbf{A}^k}{k!} \\ &= \sum_{k=0}^{\infty} \sum_{j=1}^d \frac{1}{k!} E_j^k \mathbf{u}_j \mathbf{u}_j^\dagger = \sum_{j=1}^d e^{E_j} \mathbf{u}_j \mathbf{u}_j^\dagger, \end{aligned} \quad (\text{A.5})$$

For $\theta \in \mathbb{R}$ and Hermitian \mathbf{H} , $\exp(-i\theta\mathbf{H})$ is unitary, since:

$$\exp(-i\theta\mathbf{H})^\dagger = \left(\sum_{k=0}^{\infty} \frac{(-i\theta\mathbf{H})^k}{k!} \right)^\dagger \quad (\text{A.6})$$

$$= \sum_{k=0}^{\infty} \frac{(i\theta\mathbf{H})^k}{k!} = \exp(i\theta\mathbf{H}), \quad (\text{A.7})$$

and

$$\exp(i\theta\mathbf{H}) \exp(-i\theta\mathbf{H}) = \left(\sum_{j=1}^d e^{i\theta E_j} \mathbf{u}_j \mathbf{u}_j^\dagger \right) \quad (\text{A.8})$$

$$= \left(\sum_{k=1}^d e^{-i\theta E_k} \mathbf{u}_k \mathbf{u}_k^\dagger \right) = \mathbf{I}_{d \times d}. \quad (\text{A.9})$$

Kronecker product. For $\mathbf{A} \in \mathbb{C}^{d_1 \times d_2}$ and $\mathbf{B} \in \mathbb{C}^{d_2 \times d_2}$, the Kronecker product of \mathbf{A} and \mathbf{B} is defined as:

$$\mathbf{A} \otimes \mathbf{B} = \begin{bmatrix} A_{11}\mathbf{B} & A_{12}\mathbf{B} & \cdots & A_{1d_1}\mathbf{B} \\ A_{21}\mathbf{B} & A_{22}\mathbf{B} & \cdots & A_{2d_1}\mathbf{B} \\ \vdots & \vdots & \ddots & \vdots \\ A_{d_11}\mathbf{B} & A_{d_12}\mathbf{B} & \cdots & A_{d_1d_1}\mathbf{B} \end{bmatrix} \quad (\text{A.10})$$

where A_{ij} is the (i, j) -th element of matrix \mathbf{A} . As can be seen from the definition $\mathbf{A} \otimes \mathbf{B} \in \mathbb{C}^{d_1 d_2 \times d_1 d_2}$. We also use the symbol \otimes for direct product of Hilbert spaces depending on the context.

By definition, the trace of $\mathbf{A} \otimes \mathbf{B}$

$$\text{tr}(\mathbf{A} \otimes \mathbf{B}) = \sum_{j=1}^{d_1} A_{jj} \text{tr}(\mathbf{B}) = \text{tr}(\mathbf{A}) \text{tr}(\mathbf{B}) \quad (\text{A.11})$$

A.2. Quantum Information

We now describe notions in quantum information using linear algebra. We start by formulating quantum mechanics in the language of density matrices.

Quantum states. A *quantum state* with dimension d is can be represented by a positive semidefinite (PSD) Hermitian $\rho \in \mathbb{C}^{d \times d}$, the *density matrix*. For any PSD Hermitian ρ with $\text{tr}(\rho) = 1$, there is a corresponding quantum state, and vice versa.

Quantum states with rank-1 density matrices are referred to as *pure states*. For a pure state, its density matrix ρ allows a eigen-decomposition $\rho = \mathbf{v}\mathbf{v}^\dagger$ with $\mathbf{v} \in \mathbb{C}^d$ being a ℓ_2 -unit vector. \mathbf{v} is referred to as the state vector representation of a pure quantum state.

The state space of a system composed of two subsystem with dimension d_1 and d_2 has a dimension of $d_1 d_2$. And a density matrix for a such composite system lies in $\mathbb{C}^{d_1 \times d_1} \otimes \mathbb{C}^{d_2 \times d_2}$. If a state can be expressed as a Kronecker product of density matrices, we say it is a *product state*. A simplistic example is $\rho_{12} := \rho_1 \otimes \rho_2$ with $\rho_1 \in \mathbb{C}^{d_1}$ and $\rho_2 \in \mathbb{C}^{d_2}$.

Analogous to classical binary bits, the basic element for quantum computers are *qubits*. The state space of a single qubit is 2-dimensional, and the density matrix for a system composed of n qubits lies in $\otimes_{i=1}^n \mathbb{C}^{2 \times 2}$.

Unitary gates. An operation over a quantum state is a linear map that is completely positive and preserves the trace (See (Watrous, 2018) for a rigorous definition). Throughout this paper we focus on *unitary operators*. In the context of quantum circuit models, operations are also referred to as *gates*.

Under the density matrix representation, a unitary gate, denoted by $\mathbf{U} \in \mathbb{C}^{d \times d}$, transforms a state $\rho \in \mathbb{C}^{d \times d}$ to $\rho' = \mathbf{U}\rho\mathbf{U}^\dagger$. The positive semidefiniteness and the trace are preserved. For a pure state $\rho = \mathbf{v}\mathbf{v}^\dagger$, under the state vector representation, the unitary gate \mathbf{U} transforms \mathbf{v} to $\mathbf{v}' = \mathbf{U}\mathbf{v}$.

A set of unitary gates commonly used on a qubit are the *Pauli gates*:

$$\mathbf{X} = \begin{bmatrix} 0 & 1 \\ 1 & 0 \end{bmatrix}, \mathbf{Y} = \begin{bmatrix} 0 & -i \\ i & 0 \end{bmatrix}, \mathbf{Z} = \begin{bmatrix} 1 & 0 \\ 0 & -1 \end{bmatrix}; \quad (\text{A.12})$$

Note that the Pauli gates are both unitary and Hermitian.

We are especially interested in unitary gates parameterized by $\theta \in \mathbb{R}$ as $\exp(-i\theta\mathbf{H})$ for a Hermitian \mathbf{H} . We sometimes refer to \mathbf{H} as the *Hamiltonian* that generates the parameterized quantum gate. For any $\lambda \in \mathbb{R}$, shifting \mathbf{H} by $\lambda \cdot \mathbf{I}$ does not change the parameterized gate. To see this, for any ρ , consider $\tilde{\mathbf{H}} = \mathbf{H} + \lambda\mathbf{I}$:

$$e^{-i\theta\tilde{\mathbf{H}}}\rho e^{i\theta\tilde{\mathbf{H}}} = e^{-i\theta\lambda} \cdot e^{-i\theta\mathbf{H}}\rho e^{i\theta\mathbf{H}} \cdot e^{i\theta\lambda} \quad (\text{A.13})$$

$$= e^{-i\theta\mathbf{H}}\rho e^{i\theta\mathbf{H}}. \quad (\text{A.14})$$

Quantum measurements and observables A measurement of quantum states is specified by a set of matrices $\{\mathbf{M}_m\} \subset \mathbb{C}^{d \times d}$ with $\mathbf{M}_m^\dagger \mathbf{M}_m = \mathbf{I}_{d \times d}$, and a set of outcomes $\{\lambda_m\} \subset \mathbb{R}$. Such measurements on the density matrix ρ yield the outcome λ_m with probability $\text{tr}(\mathbf{M}_m^\dagger \mathbf{M}_m \rho)$. The probabilities are normalized

$$\sum_m \text{tr}(\mathbf{M}_m^\dagger \mathbf{M}_m \rho) \quad (\text{A.15})$$

$$= \text{tr}\left(\sum_m \mathbf{M}_m^\dagger \mathbf{M}_m \rho\right) \quad (\text{A.16})$$

$$= \text{tr}(\rho) = 1. \quad (\text{A.17})$$

In this paper we mainly focus on the expected outcome of a measurement. Let \mathbf{M} denote the *observable* $\sum_m \lambda_m \mathbf{M}_m^\dagger \mathbf{M}_m$, the expected value of the outcome is

$$\sum_m \lambda_m \text{tr}(\mathbf{M}_m^\dagger \mathbf{M}_m \rho) = \text{tr}\left(\sum_m \lambda_m \mathbf{M}_m^\dagger \mathbf{M}_m \rho\right) \quad (\text{A.18})$$

$$= \text{tr}(\mathbf{M}\rho). \quad (\text{A.19})$$

B. Proofs for Constructions

In this section, we provide the detailed proof for the existence of constructions appeared in Section 3.

We start by recalling the definitions of $\Phi_l^{(j)}(\cdot)$ and summarize some useful facts about these linear maps in Subsection B.1, as well as the observables in the Heisenberg picture. In Subsection B.2 we elaborate on our result on the existence of hard datasets for p -parameter QNNs with linear independence, which leads to the following theorem:

Theorem 2 (Construction: exponentially many local minima). *Consider QNNs composed of unitaries generated by two-level Hamiltonians, parameterized by $\theta \in \mathbb{R}^p$. If the QNN is with linear independence, a dataset \mathcal{S} can be constructed to induce a loss function $L(\theta; \mathcal{S})$ with 2^p local minima within each period, and $2^p - 1$ of these minima are spurious with positive suboptimality gap.*

In Subsection B.3 we identify a family of 1-layer QNNs with linear independence, which gives rise to Proposition 5. In addition, we instantiated concrete datasets to illustrate the generality of our construction.

B.1. Linear Maps $\Phi_l^{(j)}(\cdot)$

Recall the definitions of $\Phi_l^{(j)}$: For all $l \in [p]$, define $\Phi_l^{(j)}$ such that for any Hermitian \mathbf{A} :

$$\Phi_l^{(0)}(\mathbf{A}) = \frac{1}{2}(\mathbf{A} + \mathbf{H}_l \mathbf{A} \mathbf{H}_l) \quad (\text{B.1})$$

$$\Phi_l^{(1)}(\mathbf{A}) = \frac{1}{2}(\mathbf{A} - \mathbf{H}_l \mathbf{A} \mathbf{H}_l) \quad (\text{B.2})$$

$$\Phi_l^{(2)}(\mathbf{A}) = \frac{i}{2}[\mathbf{H}_l, \mathbf{A}] \quad (\text{B.3})$$

The subscript l will be dropped for general \mathbf{H} .

It can be easily verified that these mappings maps Hermitians to Hermitians, and the traces of the output:

$$\text{tr}\left(\Phi_l^{(0)}(\mathbf{A})\right) = \text{tr}\left(\frac{\mathbf{A} + \mathbf{H}_l \mathbf{A} \mathbf{H}_l}{2}\right) = \text{tr}(\mathbf{A}) \quad (\text{B.4})$$

$$\text{tr}\left(\Phi_l^{(1)}(\mathbf{A})\right) = \text{tr}\left(\frac{\mathbf{A} - \mathbf{H}_l \mathbf{A} \mathbf{H}_l}{2}\right) = 0 \quad (\text{B.5})$$

$$\text{tr}\left(\Phi_l^{(2)}(\mathbf{A})\right) = \text{tr}\left(\frac{i[\mathbf{H}_l, \mathbf{A}]}{2}\right) = 0 \quad (\text{B.6})$$

Adjoint The adjoints of the maps are:

$$\left(\Phi_l^{(0)}\right)^*(\mathbf{A}) = \Phi_l^{(0)}(\mathbf{A}) \quad (\text{B.7})$$

$$\left(\Phi_l^{(1)}\right)^*(\mathbf{A}) = \Phi_l^{(1)}(\mathbf{A}) \quad (\text{B.8})$$

$$\left(\Phi_l^{(2)}\right)^*(\mathbf{A}) = -\Phi_l^{(2)}(\mathbf{A}) \quad (\text{B.9})$$

For all pairs of $j, k \in \{0, 1, 2\}$, we summarize the composition of mappings $(\Phi_l^{(j)})^* \circ \Phi_l^{(k)}(\cdot)$ in Table 1, and the inner products $\langle \Phi_l^{(j)}(\mathbf{A}), \Phi_l^{(k)}(\mathbf{A}) \rangle$ in Table 2.

Table 1. Composition $(\Phi_l^{(j)})^* \circ \Phi_l^{(k)}(\cdot)$

j\k	0	1	2
0	$\Phi_l^{(0)}(\cdot)$	0	0
1	0	$\Phi_l^{(1)}(\cdot)$	$\Phi_l^{(2)}(\cdot)$
2	0	$-\Phi_l^{(2)}(\cdot)$	$\Phi_l^{(1)}(\cdot)$

Table 2. Inner product $\langle \Phi_l^{(j)}(\mathbf{A}), \Phi_l^{(k)}(\mathbf{A}) \rangle$

j\k	0	1	2
0	$\langle \mathbf{A}, \Phi_l^{(0)}(\mathbf{A}) \rangle$	0	0
1	0	$\langle \mathbf{A}, \Phi_l^{(1)}(\mathbf{A}) \rangle$	0
2	0	0	$\langle \mathbf{A}, \Phi_l^{(1)}(\mathbf{A}) \rangle$

All off-diagonal elements are zero in Table 2, implying the orthogonality of $\{\Phi_l^{(j)}\}_{j=0,1,2}$. This follows from the fact

$$\langle \mathbf{A}, \Phi_l^{(2)}(\mathbf{A}) \rangle = \frac{i}{2}(\text{tr}(\mathbf{A}\mathbf{H}\mathbf{A}) - \text{tr}(\mathbf{A}^2\mathbf{H})) = 0 \quad (\text{B.10})$$

We are now ready to prove the expansion of the observable in Heisenberg picture:

Claim B.1 (Observable in Heisenberg Picture). For quantum neural networks defined in Theorem 2, the observable in Heisenberg picture $\mathbf{U}(\boldsymbol{\theta})^\dagger \mathbf{M} \mathbf{U}(\boldsymbol{\theta})$ can be expressed as:

$$\sum_{\xi \in \{0,1,2\}^p} \Phi_\xi(\mathbf{M}) \prod_{l:\xi_l=1} \cos 2\theta_l \prod_{l':\xi_{l'}=2} \sin 2\theta_{l'} \quad (\text{B.11})$$

where Φ_ξ is defined as the following composed mapping:

$$\Phi_1^{(\xi_1)} \circ \Phi_2^{(\xi_2)} \circ \dots \circ \Phi_p^{(\xi_p)} \quad (\text{B.12})$$

Proof. For a two-level Hamiltonian \mathbf{H} with eigenvalues ± 1 , let \mathbf{P}_+ and \mathbf{P}_- be projections into subspaces of \mathbb{C}^d corresponding to eigenvalues $+1$ and -1 :

$$\mathbf{H} = \mathbf{P}_+ - \mathbf{P}_-, \text{ and } \mathbf{P}_+ + \mathbf{P}_- = \mathbf{I}; \quad (\text{B.13})$$

For all $\theta \in \mathbb{R}$, the parameterized unitary

$$\exp(-i\theta\mathbf{H}) = e^{-i\theta}\mathbf{P}_+ + e^{i\theta}\mathbf{P}_- \quad (\text{B.14})$$

$$= \cos\theta(\mathbf{P}_+ + \mathbf{P}_-) - \sin\theta i(\mathbf{P}_+ - \mathbf{P}_-) \quad (\text{B.15})$$

$$= \cos\theta\mathbf{I} - i\sin\theta\mathbf{H} \quad (\text{B.16})$$

By basic trigonometry, $e^{i\theta\mathbf{H}}\mathbf{A}e^{-i\theta\mathbf{H}}$ can be expressed as

$$\Phi^{(0)}(\mathbf{A}) + \Phi^{(1)}(\mathbf{A})\cos 2\theta + \Phi^{(2)}(\mathbf{A})\sin 2\theta \quad (\text{B.17})$$

for any Hermitian \mathbf{A} . Claim B.1 then follows from sequential application of Eqn. (B.17). \square

Under transformation $\boldsymbol{\theta} \mapsto \boldsymbol{\theta} + \boldsymbol{\alpha}$ for some $\boldsymbol{\alpha} \in \mathbb{R}^p$, the linear maps transform as:

$$\begin{cases} \Phi_l^{(0)}(\cdot) & \rightarrow \Phi_l^{(0)}(\cdot) \\ \Phi_l^{(1)}(\cdot) & \rightarrow \cos 2\alpha_l \Phi_l^{(1)}(\cdot) + \sin 2\alpha_l \Phi_l^{(2)}(\cdot) \\ \Phi_l^{(2)}(\cdot) & \rightarrow -\sin 2\alpha_l \Phi_l^{(1)}(\cdot) + \cos 2\alpha_l \Phi_l^{(2)}(\cdot) \end{cases} \quad (\text{B.18})$$

This is because $e^{i(\theta+\alpha)\mathbf{H}}\mathbf{A}e^{-i(\theta+\alpha)\mathbf{H}}$ can be expressed as

$$\begin{aligned} & \Phi^{(0)}(\mathbf{A}) + (\cos 2\alpha\Phi^{(1)}(\mathbf{A}) + \sin 2\alpha\Phi^{(2)}(\mathbf{A}))\cos 2\theta \\ & + (-\sin 2\alpha\Phi^{(1)}(\mathbf{A}) + \cos 2\alpha\Phi^{(2)}(\mathbf{A}))\sin 2\theta \end{aligned} \quad (\text{B.19})$$

As a consequence, each term of $f(\boldsymbol{\rho}; \boldsymbol{\theta})$ remain invariant under the joint transformation $\theta_l \mapsto \theta_l + \frac{\pi}{2}$ and

$$\Phi_l^{(0)}(\cdot) \mapsto \mathbf{H}_l \Phi_l^{(0)}(\cdot) \mathbf{H}_l = \Phi_l^{(0)}(\cdot) \quad (\text{B.20})$$

$$\Phi_l^{(1)}(\cdot) \mapsto \mathbf{H}_l \Phi_l^{(1)}(\cdot) \mathbf{H}_l = -\Phi_l^{(1)}(\cdot) \quad (\text{B.21})$$

$$\Phi_l^{(2)}(\cdot) \mapsto \mathbf{H}_l \Phi_l^{(2)}(\cdot) \mathbf{H}_l = -\Phi_l^{(2)}(\cdot) \quad (\text{B.22})$$

B.2. Proof for Lemma 3 and 4

The construction for Theorem 2 consists of two steps. For the first step, dataset \mathcal{S}_0 is constructed with 2^p local minima invariant under the $\frac{\pi}{2}$ translational symmetry:

$$\theta_l \mapsto \theta_l + \frac{\pi}{2}. \quad (\text{B.23})$$

Therefore the existence of a single local minimum $\boldsymbol{\theta}^*$ indicates a set of local minima Θ . For the second step, we construct a data set \mathcal{S}_1 to break the symmetry. A combination of these two data set with proper scaling gives us a desired dataset for Theorem 2.

Here we provide the proof of Lemma 3 and Lemma 4 in details.

Lemma 3 (Creating symmetry). *For QNNs with linear independence as mentioned in Theorem 2, a dataset \mathcal{S}_0 can be constructed to induce a loss function $L(\boldsymbol{\theta}; \mathcal{S}_0)$ that (1) has a local minimum at some $\boldsymbol{\theta}^*$, and (2) is invariant under translation $\theta_l \mapsto \theta_l + \frac{\pi}{2}$ for all $l \in [p]$.*

Proof. It suffices to construct a dataset $\mathcal{S}_0 = \{(\boldsymbol{\rho}_k, y_k)\}_{k=1}^{m_0}$, such that (1) for all $k \in [p]$, $f_k(\boldsymbol{\theta}) := \langle \boldsymbol{\rho}_k, \mathbf{M}(\boldsymbol{\theta}) \rangle - y_k$ is either symmetric or anti-symmetric under $\theta_l \mapsto \theta_l + \frac{\pi}{2}$ for all $l \in [p]$, and (2) the intersection Θ of the set of roots Θ_k of $f_k(\boldsymbol{\theta}) = 0$ is non-empty and contains at least one isolated point $\boldsymbol{\theta}^*$. For such \mathcal{S}_0 , $\boldsymbol{\theta}^*$ is an isolated root of the non-negative loss function $L(\boldsymbol{\theta}; \mathcal{S}_0) = \sum_{k=1}^{m_0} f_k(\boldsymbol{\theta})^2$.

For a concrete construction, consider $\{f_k(\boldsymbol{\theta})\}_{k=1}^{m_0}$ such that $f_k(\boldsymbol{\theta}) = \alpha \sin(2 \sum_{l=1}^p \eta_l^{(k)} (\theta_l - \theta_l^*))$ for a set of vectors $\{\boldsymbol{\eta}^{(k)}\}_{k=1}^{m_0} \subseteq \{-1, 0, 1\}^p$ that spans \mathbb{R}^p , and arbitrary $\boldsymbol{\theta}^* \in \mathbb{R}^p$.

The translational symmetry holds due to the periodicity of sin-functions; the loss function has a minima at the vanishing point $\boldsymbol{\theta}^*$.

To see that $\boldsymbol{\theta}^*$ is indeed a isolated minima (that there exists a neighbourhood within which the loss function vanishes only at $\boldsymbol{\theta}^*$), consider $\mathcal{N}(\boldsymbol{\theta}^*) := \{\boldsymbol{\theta} \in \mathbb{R}^p : \forall k \in [m_0], |(\boldsymbol{\eta}^{(k)})^T(\boldsymbol{\theta} - \boldsymbol{\theta}^*)| < \frac{\pi}{4}\}$. Conditioned on $\boldsymbol{\theta} \in \mathcal{N}(\boldsymbol{\theta}^*)$,

$$L(\boldsymbol{\theta}; \mathcal{S}_0) = 0 \implies \quad (\text{B.24})$$

$$\forall k \in [m_0], \sum_{l=1}^p \eta_l^{(k)} (\theta_l - \theta_l^*) = 0 \quad (\text{B.25})$$

which then implies $\boldsymbol{\theta} = \boldsymbol{\theta}^*$ since $\{\boldsymbol{\eta}_k^{(l)}\}_{l=1}^p$ spans \mathbb{R}^p .

The existence of such dataset \mathcal{S}_0 follows from the linear independence of operators for the QNN: for any $k \in [m_0]$, the solution set to the following linear system for Hermitian $\mathbf{D}_k \in \mathbb{C}^{d \times d}$ is non-empty:

$$\begin{cases} \langle \mathbf{D}_k, \mathbf{I} \rangle = 0, \\ \langle \mathbf{D}_k, \Phi_{\boldsymbol{\xi}}(\mathbf{M}) \rangle = \hat{f}_{\boldsymbol{\xi}, k}, \quad \forall \boldsymbol{\xi} \neq \mathbf{0}. \end{cases} \quad (\text{B.26})$$

where \mathbf{I} is the d -dimensional identity, and $\hat{f}_{\boldsymbol{\xi}, k}$ denotes the coefficient corresponding to the term $\prod_{l: \xi_l=1} \cos 2\theta_l \prod_{l': \xi_{l'}=2} \sin 2\theta_{l'}$ in $\sin(2 \sum_{l=1}^p \eta_l^{(k)} (\theta_l - \theta_l^*))$.

As $\text{tr}(\Phi_{\boldsymbol{\xi}}(\mathbf{M})) = 0$, \mathbf{I} is orthogonal to all $\Phi_{\boldsymbol{\xi}}(\mathbf{M})$. Therefore the constraint set $\{\Phi_{\boldsymbol{\xi}}(\mathbf{M})\}_{\boldsymbol{\xi} \neq \mathbf{0}} \cup \{\mathbf{I}\}$ is linear independent. As a result, the linear system is guaranteed to have a set of solution $\{\mathbf{D}_k\}_{k=1}^{m_0}$.

Given the solution $\{\mathbf{D}_k\}_{k=1}^{m_0}$, the dataset can be constructed as:

$$\boldsymbol{\rho}_k := \frac{1}{d} \mathbf{I} + \kappa \mathbf{D}_k, \quad y_k = \text{tr}(\boldsymbol{\rho}_k \Phi_0(\mathbf{M})) \quad (\text{B.27})$$

for all k , with κ be the largest positive real number such that $\frac{1}{d} \mathbf{I} + \kappa \mathbf{D}_k$ is positive semidefinite.

It can be verified by elementary calculation that such dataset yields a loss function $L(\boldsymbol{\theta}; \mathcal{S}_0) = \kappa \sum_{k=1}^{m_0} \sin(2(\boldsymbol{\eta}^{(k)})^T(\boldsymbol{\theta} - \boldsymbol{\theta}^*))$. \square

Lemma 4 (Breaking symmetry). *Consider the QNN, dataset \mathcal{S}_0 and local minimum $\boldsymbol{\theta}^*$ defined in Lemma 3. Let Θ denote the set of 2^p local minima due to the translational invariance. There exists a dataset \mathcal{S}_1 such that*

$$\inf_{\boldsymbol{\theta} \in \mathcal{N}(\boldsymbol{\theta}^*)} L(\boldsymbol{\theta}; \mathcal{S}_0) + L(\boldsymbol{\theta}; \mathcal{S}_1) < \inf_{\boldsymbol{\theta} \in \mathcal{N}(\boldsymbol{\theta}')} L(\boldsymbol{\theta}; \mathcal{S}_0) + L(\boldsymbol{\theta}; \mathcal{S}_1) \quad (\text{16})$$

for all $\boldsymbol{\theta}' \in \Theta \setminus \{\boldsymbol{\theta}^*\}$, and that

$$L(\boldsymbol{\theta}; \mathcal{S}_0) + L(\boldsymbol{\theta}; \mathcal{S}_1) > L(\boldsymbol{\theta}'; \mathcal{S}_0) + L(\boldsymbol{\theta}'; \mathcal{S}_1) \quad (\text{17})$$

for all $\boldsymbol{\theta}' \in \Theta$ and all $\boldsymbol{\theta} \in \partial \mathcal{N}(\boldsymbol{\theta}')$. Here $\mathcal{N}(\cdot)$ denote a bounded and closed neighbourhood, such that $\mathcal{N}(\boldsymbol{\theta}) \cap \mathcal{N}(\boldsymbol{\theta}') = \emptyset$ for any $\boldsymbol{\theta}, \boldsymbol{\theta}' \in \Theta$. And let $\partial \mathcal{N}$ denote its boundary.

Proof. Rewrite the loss function induced by \mathcal{S}_1 as:

$$L(\boldsymbol{\theta}; \mathcal{S}_1) = -\frac{2}{m_1} \sum_{k=1}^{m_1} \langle y_k \boldsymbol{\rho}_k, \mathbf{M}(\boldsymbol{\theta}) \rangle \quad (\text{B.28})$$

$$+ \frac{1}{m_1} \sum_{k=1}^{m_1} (\langle \boldsymbol{\rho}_k, \mathbf{M}(\boldsymbol{\theta}) \rangle)^2 \quad (\text{B.29})$$

$$+ \frac{1}{m_1} \sum_{k=1}^{m_1} y_k^2 \quad (\text{B.30})$$

For any positive ϵ , consider the following joint scaling of $\boldsymbol{\rho}_k$ and y_k :

$$\begin{cases} \boldsymbol{\rho}_k \mapsto \epsilon \boldsymbol{\rho}_k + (1 - \epsilon) \frac{1}{d} \mathbf{I} \\ y_k \mapsto \frac{1}{\epsilon} y_k \end{cases} \quad (\text{B.31})$$

Under such scaling, for arbitrary ϵ , term (B.28) remains the same; the term (B.29) can be arbitrarily suppressed by choosing sufficiently small ϵ . Therefore it suffices to consider the first term $L'(\cdot; \mathcal{S}_1) := -\frac{2}{m_1} \sum_{k=1}^{m_1} y_k \langle \boldsymbol{\rho}_k, \mathbf{M}(\boldsymbol{\theta}) \rangle$.

Without loss of generality, assume $\boldsymbol{\theta}^* = \mathbf{0}$. Consider a dataset \mathcal{S}_1 such that $L'(\boldsymbol{\theta}; \mathcal{S}_1) \propto -\sum_{k=1}^{m_1} \cos(2(\tilde{\boldsymbol{\eta}}^{(k)})^T \boldsymbol{\theta})$ for a set $\{\tilde{\boldsymbol{\eta}}^{(k)}\}_{k=1}^{m_1} \subset \{0, 1\}^p$ that spans $\{0, 1\}^p$.

For any $\boldsymbol{\zeta} \in \{0, 1\}^p$,

$$L'(\boldsymbol{\theta}^* + \frac{\pi}{2} \boldsymbol{\zeta}; \mathcal{S}_1) \quad (\text{B.32})$$

$$\propto -\sum_{k=1}^{m_1} \cos(2(\tilde{\boldsymbol{\eta}}^{(k)})^T \boldsymbol{\theta}^* + \langle \tilde{\boldsymbol{\eta}}^{(k)}, \boldsymbol{\zeta} \rangle \pi) \quad (\text{B.33})$$

$$\propto -\sum_{k=1}^{m_1} (-1)^{\langle \tilde{\boldsymbol{\eta}}^{(k)}, \boldsymbol{\zeta} \rangle} \quad (\text{B.34})$$

The fact that $\{\tilde{\boldsymbol{\eta}}^{(k)}\}_{k=1}^{m_1}$ spans $\{0, 1\}^p$ indicate that the solution to

$$\forall k \in [m_1], \langle \tilde{\boldsymbol{\eta}}^{(k)}, \boldsymbol{\zeta} \rangle = 0 \pmod{2} \quad (\text{B.35})$$

is unique. Therefore such \mathcal{S}_1 breaks the $\pi/2$ -translational symmetry as required. Similar to the proof of Lemma 3, the existence of such dataset follows from the linear independence of the operators.

For a concrete construction, let \mathcal{S}_1 be a dataset such that $L'(\boldsymbol{\theta}; \mathcal{S}_1) = -\frac{2}{m_1} \sum_{k=1}^{m_1} \langle y_k \boldsymbol{\rho}_k, \mathbf{M}(\boldsymbol{\theta}) \rangle =$

$-c \sum_{l=1}^p \cos(\theta_l)$. Due to the flexible scaling of the labels $\{y_k\}_{k=1}^{m_1}$, such \mathcal{S}_1 can be found for arbitrary c .

Let $\mathcal{B}_r(\boldsymbol{\theta})$ denote the closed ℓ_2 -ball centered at $\boldsymbol{\theta}$ with radius r , and let $\partial\mathcal{B}_r$ denote its boundary. For the local minimum $\boldsymbol{\theta}^*$ of $L(\boldsymbol{\theta}; \mathcal{S}_0)$, let (r, L_0) be a pair of real numbers such that $\inf_{\boldsymbol{\theta} \in \partial\mathcal{B}_r(\boldsymbol{\theta}^*)} L(\boldsymbol{\theta}; \mathcal{S}_0) > L_0$ for some positive real number L_0 .

The requirements in Lemma 4 is then met by choosing $c < \frac{L_0}{2pr^2}$. To see this we will make use of the estimation $1 - \frac{1}{2}\theta_l^2 \leq \cos \theta_l \leq 1$. For any $\boldsymbol{\theta}' \in \Theta$, the loss function $L(\boldsymbol{\theta}; \mathcal{S}_0) + L'(\boldsymbol{\theta}; \mathcal{S}_1)$ evaluated at all points on the boundary of $B_r(\boldsymbol{\theta}')$ is at least $\frac{L_0}{2}$ larger than $L(\boldsymbol{\theta}', \mathcal{S}_0) + L'(\boldsymbol{\theta}', \mathcal{S}_1)$. Therefore the second requirement in Lemma 4 is met.

For the first requirement, we have that (1) $L(\boldsymbol{\theta}^*; \mathcal{S}_0) + L'(\boldsymbol{\theta}^*; \mathcal{S}_0) = -pc$, and (2) for all $\boldsymbol{\theta}' \in \Theta \setminus \{\boldsymbol{\theta}^*\}$, for all $\boldsymbol{\theta} \in \mathcal{B}_r(\boldsymbol{\theta}')$, $L(\boldsymbol{\theta}; \mathcal{S}_0) + L'(\boldsymbol{\theta}; \mathcal{S}_0) > 0 - (p-1)c + (1 - \frac{1}{2}r^2)c = -pc + (2 - \frac{1}{r^2})c$. The suboptimality gap is therefore at least $c(2 - \frac{1}{r^2})$. \square

Remarks. In the proof for Lemma 3 and 4, we made use of specific forms of sin- and cos-functions for the clarity of proof. However, the linear independence of the operators allow us to construct loss function beyond these specific forms, as will be made clear in Example 2 and 3.

B.3. Proof for Proposition 5 and Concrete Constructions

Proposition 5 (One-layer QNNs with product observables). *Consider the family of QNNs composed of unitaries generated by two-level Hamiltonians, parameterized by $\boldsymbol{\theta} \in \mathbb{R}^p$. For all $l \in [p]$, let \mathbf{H}_l be a local Hamiltonian on the l -qubit, taking the form $\mathbf{I} \otimes \dots \otimes \mathbf{h}_l \otimes \dots \otimes \mathbf{I}$ for some Hermitian \mathbf{h}_l at the l -th position, and $\mathbf{M} = \mathbf{m}_1 \otimes \dots \otimes \mathbf{m}_p$ such that $\mathbf{m}_l + \mathbf{h}_l \mathbf{m}_l \mathbf{h}_l$ and $\mathbf{m}_l - \mathbf{h}_l \mathbf{m}_l \mathbf{h}_l$ are non-zero for any l . There exists a dataset that induces a loss function with $2^p - 1$ spurious local minima.*

Proof. Proposition 5 follows directly from the orthogonality of the operators. For any $\boldsymbol{\xi} \in \{0, 1, 2\}^p$, the operator $\Phi_{\boldsymbol{\xi}}(\mathbf{M})$ can be expressed in the tensor product form $\otimes_{l=1}^p \tilde{\Phi}_l^{(\xi_l)}(\mathbf{m}_l)$, where $\tilde{\Phi}_l^{(j)}$ are linear maps associated with \mathbf{h}_l . For any $\boldsymbol{\xi}$ and $\boldsymbol{\xi}' \in \{0, 1, 2\}^p \setminus \mathbf{0}$:

$$\langle \Phi_{\boldsymbol{\xi}}(\mathbf{M}), \Phi_{\boldsymbol{\xi}'}(\mathbf{M}) \rangle \quad (\text{B.36})$$

$$= \prod_{l=1}^p \langle \tilde{\Phi}_l^{(\xi_l)}(\mathbf{m}_l), \tilde{\Phi}_l^{(\xi'_l)}(\mathbf{m}_l) \rangle \quad (\text{B.37})$$

$$= \prod_{l=1}^p \|\tilde{\Phi}_l^{(\xi_l)}(\mathbf{m}_l)\|_F^2 \delta_{\xi_l, \xi'_l} \quad (\text{B.38})$$

Therefore $\{\Phi_{\boldsymbol{\xi}}(\mathbf{M})\}$ forms a linear independent set. \square

We now move on to concrete constructions of datasets for QNNs defined in Proposition 5. To facilitate narrative, assume $\mathbf{M} = \mathbf{M}_0^{\otimes p}$, and $\mathbf{h}_l = \mathbf{H}_0$.

For $j = 0, 1, 2$, define $\mathbf{D}^{(j)}$ as $\Phi^{(j)}(\mathbf{M}_0)$. And let $\boldsymbol{\rho}^{(j)}$ be a proper linear combination of $\mathbf{D}^{(j)}$ and \mathbf{I} that is positive semidefinite and trace-1.

For $l \in [p]$, define

$$\boldsymbol{\rho}_{0,l} = (\otimes_{r=1}^{l-1} \boldsymbol{\rho}^{(0)}) \otimes \boldsymbol{\rho}^{(1)} \otimes (\otimes_{r=l+1}^p \boldsymbol{\rho}^{(0)}) \quad (\text{B.39})$$

$$\boldsymbol{\rho}_{1,l} = (\otimes_{r=1}^{l-1} \boldsymbol{\rho}^{(0)}) \otimes \boldsymbol{\rho}^{(2)} \otimes (\otimes_{r=l+1}^p \boldsymbol{\rho}^{(0)}) \quad (\text{B.40})$$

$$y_{0,l} = 0 \quad (\text{B.41})$$

$$y_{1,l} = \text{tr}(\boldsymbol{\rho}^{(0)} \Phi^{(0)}(\mathbf{M}_0))^{p-1} \text{tr}(\boldsymbol{\rho}^{(1)} \Phi^{(1)}(\mathbf{M}_0)) \quad (\text{B.42})$$

Let $\mathcal{S}_0 = \{(\boldsymbol{\rho}_{0,l}, y_{0,l})\}_{l=1}^p$ be the dataset with $\frac{\pi}{2}$ -translational symmetry, with the resulting loss function proportional to $\sum_{l=1}^p \sin^2 \theta_l^2$; Let $\mathcal{S}_1 = \{(\boldsymbol{\rho}_{1,l}, y_{1,l})\}_{l=1}^p$ be the dataset that breaks the symmetry, with the loss function proportional to $\sum_{l=1}^p (\cos \theta_l - 1)^2$.

Example 1. For a concrete example, consider $\mathbf{M}_0 = \mathbf{Y} + \mathbf{I}$, and $\mathbf{H}_0 = \mathbf{Z}$. Choose $\boldsymbol{\rho}^{(0)} = \frac{1}{2}(\mathbf{Z} + \mathbf{I})$, $\boldsymbol{\rho}^{(1)} = \frac{1}{2}(\mathbf{X} + \mathbf{I})$, $\boldsymbol{\rho}^{(2)} = \frac{1}{2}(\mathbf{Y} + \mathbf{I})$. Construct the dataset \mathcal{S}_0 and \mathcal{S}_1 as described above, and let the dataset \mathcal{S} be the combination of \mathcal{S}_0 and \mathcal{S}_1 with reweighting factor 4 : 1. The loss function takes the form:

$$\frac{1}{2p} \sum_{l=1}^p \sin^2(2\theta_l) + \frac{1}{4} (\cos 2\theta_l - 1)^2 \quad (\text{B.43})$$

For clarity, the construction in Example 1 was purposefully designed with two limitations. First of all, the construction has a fixed global minima at $\boldsymbol{\theta}^* = \mathbf{0}$. Also, the loss function of the construction in Example 1 can be decomposed into p single-parameter functions. Therefore the training problem can be solved by greedily optimizing each of the coordinate θ_l .

To address the first limitation, we propose the following example:

Example 2. For

$$\boldsymbol{\rho}_{0,l} = (\otimes_{r=1}^{l-1} \boldsymbol{\rho}^{(0)}) \otimes \boldsymbol{\rho}^{(1)} \otimes (\otimes_{r=l+1}^p \boldsymbol{\rho}^{(0)}) \quad (\text{B.44})$$

$$\boldsymbol{\rho}_{1,l} = (\otimes_{r=1}^{l-1} \boldsymbol{\rho}^{(0)}) \otimes \boldsymbol{\rho}^{(2)} \otimes (\otimes_{r=l+1}^p \boldsymbol{\rho}^{(0)}) \quad (\text{B.45})$$

$$y_{0,l} = \sin\left(\frac{\pi}{50}\right), \quad y_{1,l} = \cos\left(\frac{\pi}{50}\right) \quad (\text{B.46})$$

Construct dataset $\mathcal{S}_0, \mathcal{S}_1$ as:

$$\mathcal{S}_0 = \{(\boldsymbol{\rho}_{0,l}, y_{0,l})\}_{l=1}^p, \quad \mathcal{S}_1 = \{(\boldsymbol{\rho}_{1,l}, y_{1,l})\}_{l=1}^p \quad (\text{B.47})$$

and let the dataset \mathcal{S} be the combination of \mathcal{S}_0 and \mathcal{S}_1 with

reweighting factor 4 : 1. The loss function takes the form:

$$\frac{1}{2p} \sum_{l=1}^p \left((\sin 2\theta_l - \sin \frac{\pi}{50})^2 + \frac{1}{4} (\cos 2\theta_l - \cos \frac{\pi}{50})^2 \right). \quad (\text{B.48})$$

The resulting loss function has a local minimum at $(\frac{\pi}{100}, \dots, \frac{\pi}{100})^T$.

To address the decomposability issue, consider the following example:

Example 3. Let $\mathcal{S}_0, \mathcal{S}_1$ be as defined in Example 2. Let $\rho_{2,l,k}$ denote a product state with $\rho^{(1)}$ for the k -th and l -th qubits, and $\rho^{(0)}$ for the rest. The loss function for training sample $(\rho_{2,l,k}, \cos^2 \frac{\pi}{50})$ is $(\cos 2\theta_l \cos 2\theta_k - \cos^2 \frac{\pi}{50})^2$. Combining this additional term with \mathcal{S}_0 and \mathcal{S}_1 gives rise to non-decomposable loss functions that cannot be solved by optimizing each coordinate independently.

As will be seen in S.M. Sect. E, the construction of Example 2 and 3 indicates that our construction method is general, and can lead to instances that are hard to optimize with gradient-based methods and do not admit other trivial optimization methods.

C. Proof for Typical QNNs with Linear Dependence

In this section, we show that typical under-parameterized QNNs are with linear independence. To that end, we consider random d -dimensional p -parameter QNNs sampled with respect to the following measure:

Let \mathbf{H} be a d -dimension Hermitian such that $\text{tr}(\mathbf{H}) = 0$ and $\mathbf{H}^2 = \mathbf{I}$. The circuit for our random QNN is:

$$\mathbf{U}(\theta) = e^{-i\theta_p \mathbf{W}_p \mathbf{H} \mathbf{W}_p^\dagger} \dots e^{-i\theta_1 \mathbf{W}_1 \mathbf{H} \mathbf{W}_1^\dagger} \quad (\text{C.1})$$

with $\{\mathbf{W}_l\}_{l=1}^p$ independently sampled with respect to the Haar measure on the d -dimensional unitary group $U(d)$.

Following from the fact $e^{-i\theta \mathbf{W} \mathbf{H} \mathbf{W}^\dagger} = \mathbf{W} e^{-i\theta \mathbf{H}} \mathbf{W}^\dagger$ for Hermitian \mathbf{H} and unitary \mathbf{W} , we can rewrite Eqn. (C.1) as:

$$\mathbf{U}(\theta) = \mathbf{W}_p e^{-i\theta_p \mathbf{H}} (\mathbf{W}_p^\dagger \mathbf{W}_{p-1}) \dots (\mathbf{W}_2^\dagger \mathbf{W}_1) e^{-i\theta_1 \mathbf{H}} \mathbf{W}_1^\dagger \quad (\text{C.2})$$

Due to the left (and right) invariance of the Haar measure, up to a unitary transformation, the random model in Eqn. (C.1) is equivalent to a circuit with p interleaving parameterized gate $\{e^{-i\theta_l \mathbf{H}}\}_{l=1}^p$ and unitary $\{\tilde{\mathbf{W}}_l\}_{l=1}^p$ randomly sampled with respect to the Haar measure:

$$\mathbf{U}(\theta) = \tilde{\mathbf{W}}_p e^{-i\theta_p \mathbf{H}} \tilde{\mathbf{W}}_{p-1} \dots \tilde{\mathbf{W}}_1 e^{-i\theta_1 \mathbf{H}} \quad (\text{C.3})$$

This interleaving nature of fixed and parameterized gates is shared by existing designs of QNNs, and any p -parameter QNN generated by two-level Hamiltonians can be expressed in Eqn. (C.3). Moreover, applying polynomially many random 2-qubit gates on random pairs of qubits generates a distribution over gates that approximates the Haar measure up to the 4-th moments (Brandao et al., 2016), which is what we require in the proof in this section.

In the rest of this section, we provide detailed proof for Theorem 6.

Theorem 6 (Typical under-parameterized QNNs are with linear independence). *Consider a random p -parameter d -dimensional QNN with two-level Hamiltonians sampled from the model specified in Eqn. (21). Let the observable \mathbf{M} be an arbitrary non-zero trace-0 Hermitian. Such QNN is with linear independence with probability $\geq 1 - O(d^{-1})$ for fixed p , and with probability $\geq 1 - O(e^{-p})$ for dimension $d : \log(d) = \Theta(p)$.*

C.1. Proof of Theorem 6

Proof. Let $\Xi = \{0, 1, 2\}^p / \{\mathbf{0}\}$ denote the set of all $\xi \in \{0, 1, 2\}^p$ except for $\xi = (0, \dots, 0)^T$. Our goal is to show that $\{\Phi_\xi\}_{\xi \in \Xi}$ is linearly independent with high probability.

To show the linear independence of $\{\Phi_\xi\}$, it suffices to show that its Gram matrix is positive semidefinite (Theorem 7.2.10 in Horn & Johnson (2013)). The Gram matrix \mathbf{G} is defined such that the (ξ, ξ') -element $G_{\xi, \xi'} := \langle \Phi_\xi(\mathbf{M}), \Phi_{\xi'}(\mathbf{M}) \rangle$, for all pairs of $\xi, \xi' \in \Xi$.

By the Gershgorin circle theorem (Golub & Van Loan, 1996), it suffices to show that with high probability

$$\langle \Phi_\xi(\mathbf{M}), \Phi_\xi(\mathbf{M}) \rangle > \sum_{\xi' \in \Xi, \xi' \neq \xi} |\langle \Phi_\xi(\mathbf{M}), \Phi_{\xi'}(\mathbf{M}) \rangle| \quad (\text{C.4})$$

for all $\xi \in \Xi$.

Using the Chebyshev inequality with the moment estimations in Lemma 8, we have:

$$\Pr \left[\text{tr}(\Phi_\xi(\mathbf{M})^2) < \frac{2}{3} \frac{\text{tr}(\mathbf{M}^2)}{2^p} \right] \leq O(d^{-1}) \quad (\text{C.5})$$

and

$$\Pr \left[|\text{tr}(\Phi_\xi(\mathbf{M}) \Phi_{\xi'}(\mathbf{M}))| > \frac{1}{3 \cdot 3^p} \frac{\text{tr}(\mathbf{M}^2)}{2^p} \right] \leq O(3^p d^{-1}) \quad (\text{C.6})$$

for $\xi \neq \xi'$. Combined with the union bound, we can show

that:

$$\Pr(\exists \xi \in \Xi : \langle \Phi_\xi(\mathbf{M}) \Phi_\xi(\mathbf{M}) \rangle \leq \sum_{\xi' \in \Xi: \xi' \neq \xi} |\langle \Phi_\xi(\mathbf{M}) \Phi_{\xi'}(\mathbf{M}) \rangle|) \leq O(e^p d^{-1}) \quad (\text{C.7})$$

□

C.2. Moments

Lemma 8 (Expectations and variances). *Consider the set of operators $\{\Phi_\xi(\mathbf{M})\}$ of random d -dimensional p -parameter QNNs defined in Eqn. (C.1). The expectations of diagonal and off-diagonal terms of the associated Gram matrix are:*

$$\mathbb{E}[\text{tr}(\Phi_\xi(\mathbf{M}) \Phi_\xi(\mathbf{M}))] = \frac{\text{tr}(\mathbf{M}^2)}{2^p} (1 + O(pd^{-2})) \quad (\text{C.8})$$

$$\mathbb{E}[\text{tr}(\Phi_\xi(\mathbf{M}) \Phi_{\xi'}(\mathbf{M}))] = 0 \quad (\text{C.9})$$

$$(\text{C.10})$$

for all $\xi \in \Xi$ and $\xi' \neq \xi$. The variances are:

$$\mathbb{V}[\text{tr}(\Phi_\xi(\mathbf{M}) \Phi_{\xi'}(\mathbf{M}))] = \frac{\text{tr}(\mathbf{M}^2)^2}{4^p} O(d^{-1}) \quad (\text{C.11})$$

for all $\xi, \xi' \in \Xi$.

Proof. Throughout the proof, we will use $\mathbb{E}_l[\cdot]$ to denote expectation with respect to \mathbf{H}_l , and use $\mathbb{E}_{l:p}[\cdot]$ to denote integral over the product measure over $\mathbf{W}_l, \dots, \mathbf{W}_p$. The subscripts will be dropped when there is no confusion.

We start by showing some basic (in-)equalities using the formula for integrals over the Haar measure (Puchała & Miszczak, 2011). Recall that $\mathbf{H}_l = \mathbf{W}_l \mathbf{H} \mathbf{W}_l^\dagger$. Let \mathbf{A} and \mathbf{B} be two Hermitian matrices such that $\text{tr}(\mathbf{A}) = \text{tr}(\mathbf{B}) = 0$. For integrals where \mathbf{H}_l appears once:

$$\mathbb{E}_l[\text{tr}(\mathbf{A} \mathbf{H}_l)] = \frac{1}{d} \text{tr}(\mathbf{A}) \text{tr}(\mathbf{H}) = 0 \quad (\text{C.12})$$

For integrals where \mathbf{H}_l appears twice, we have:

$$\mathbb{E}_l[\text{tr}(\mathbf{A} \mathbf{H}_l) \text{tr}(\mathbf{B} \mathbf{H}_l)] \quad (\text{C.13})$$

$$= \frac{\text{tr}(\mathbf{A} \mathbf{B}) \text{tr}(\mathbf{H}^2) + \text{tr}(\mathbf{A}) \text{tr}(\mathbf{B}) \text{tr}(\mathbf{H})^2}{d^2 - 1} \quad (\text{C.14})$$

$$- \frac{\text{tr}(\mathbf{A} \mathbf{B}) \text{tr}(\mathbf{H})^2 + \text{tr}(\mathbf{A}) \text{tr}(\mathbf{B}) \text{tr}(\mathbf{H}^2)}{d(d^2 - 1)} \quad (\text{C.15})$$

$$= \frac{1}{d - d^{-1}} \text{tr}(\mathbf{A} \mathbf{B}) \quad (\text{C.16})$$

$$\mathbb{E}_l[\text{tr}(\mathbf{A} \mathbf{H}_l \mathbf{B} \mathbf{H}_l)] \quad (\text{C.17})$$

$$= \frac{\text{tr}(\mathbf{A} \mathbf{B}) \text{tr}(\mathbf{H})^2 + \text{tr}(\mathbf{A}) \text{tr}(\mathbf{B}) \text{tr}(\mathbf{H}^2)}{d^2 - 1} \quad (\text{C.18})$$

$$- \frac{\text{tr}(\mathbf{A} \mathbf{B}) \text{tr}(\mathbf{H}^2) + \text{tr}(\mathbf{A}) \text{tr}(\mathbf{B}) \text{tr}(\mathbf{H})^2}{d(d^2 - 1)} \quad (\text{C.19})$$

$$= - \frac{1}{d^2 - 1} \text{tr}(\mathbf{A} \mathbf{B}) \quad (\text{C.20})$$

For integrals with \mathbf{H}_l appearing 4 times, we use the following estimation

$$|\mathbb{E}[\text{tr}(\mathbf{A} \mathbf{H}_l \mathbf{A} \mathbf{H}_l) \text{tr}(\mathbf{B} \mathbf{H}_l \mathbf{B} \mathbf{H}_l)]| \quad (\text{C.21})$$

$$= O(d^{-4}) \max\{|\text{tr}(\mathbf{H}^2)|^2, |\text{tr}(\mathbf{H}^4)|\} \quad (\text{C.22})$$

$$\cdot \max\{|\text{tr}(\mathbf{A}^2 \mathbf{B}^2)|, |\text{tr}(\mathbf{A} \mathbf{B} \mathbf{A} \mathbf{B})|\}, \quad (\text{C.23})$$

$$|\text{tr}(\mathbf{A} \mathbf{B})^2|, |\text{tr}(\mathbf{A}^2) \text{tr}(\mathbf{B}^2)|\} \quad (\text{C.24})$$

$$= O(d^{-2}) \text{tr}(\mathbf{A}^2) \text{tr}(\mathbf{B}^2) \quad (\text{C.25})$$

Here the first relation follows from formula on Equation (3) in (Puchała & Miszczak, 2011) and expressions in Sec. 6 of (Collins & Śniady, 2006); and the second relation follows from matrix Cauchy-Schwarz inequalities and trace inequalities from (Petz & Żemánek, 1988; Petz, 1994).

Similarly we have: $|\mathbb{E}[\text{tr}(\mathbf{A} \mathbf{H}_l \mathbf{B} \mathbf{H}_l) \text{tr}(\mathbf{A} \mathbf{H}_l \mathbf{B} \mathbf{H}_l)]| = O(d^{-2}) \text{tr}(\mathbf{A}^2) \text{tr}(\mathbf{B}^2)$.

First moments We start by calculating the first moments of $\langle \Phi_\xi(\mathbf{M}), \Phi_\xi(\mathbf{M}) \rangle$ and $\langle \Phi_\xi(\mathbf{M}), \Phi_{\xi'}(\mathbf{M}) \rangle$.

$$\mathbb{E}\langle \Phi_\xi(\mathbf{M}), \Phi_{\xi'}(\mathbf{M}) \rangle \quad (\text{C.26})$$

$$= \mathbb{E}\langle \Phi_1^{(\xi_1)} \circ \Phi_{\xi_{2:p}}(\mathbf{M}), \Phi_1^{(\xi'_1)} \circ \Phi_{\xi'_{2:p}}(\mathbf{M}) \rangle \quad (\text{C.27})$$

$$= \mathbb{E}\langle \Phi_{\xi_{2:p}}(\mathbf{M}), (\Phi_1^{(\xi_1)})^* \circ \Phi_1^{(\xi'_1)} \circ \Phi_{\xi'_{2:p}}(\mathbf{M}) \rangle \quad (\text{C.28})$$

By the basic results on the adjoints in S.M. Sect. B.1, $(\Phi_l^{(\xi_l)})^* \circ \Phi_l^{(\xi'_l)}(\cdot) = \Phi_l^{(0)}(\cdot)$ (or $\Phi_l^{(1)}(\cdot)$) if $\xi_l = \xi'_l = 0$ (or $\xi_l = \xi'_l \neq 0$). In the case $\xi_l \neq \xi'_l$, if ξ_l and ξ'_l are both in $\{1, 2\}$, $(\Phi_l^{(\xi_l)})^* \circ \Phi_l^{(\xi'_l)}(\cdot) = \pm \Phi_l^{(2)}(\cdot)$. Otherwise $(\Phi_l^{(\xi_l)})^* \circ \Phi_l^{(\xi'_l)}(\cdot) = 0$. We treat these three cases separately.

Case 1: $\xi_1 = \xi'_1$.

$$(C.26) \quad (\text{C.29})$$

$$= \mathbb{E}\langle \Phi_{\xi_{2:p}}(\mathbf{M}), \Phi_1^{(0/1)} \circ \Phi_{\xi'_{2:p}}(\mathbf{M}) \rangle \quad (\text{C.30})$$

$$= \frac{1}{2} \mathbb{E}_{2:p} \langle \Phi_{\xi_{2:p}}(\mathbf{M}), \Phi_{\xi'_{2:p}}(\mathbf{M}) \rangle \quad (\text{C.31})$$

$$\pm \frac{1}{2} \mathbb{E}\langle \Phi_{\xi_{2:p}}(\mathbf{M}), \mathbf{H}_1 \Phi_{\xi'_{2:p}}(\mathbf{M}) \mathbf{H}_1 \rangle \quad (\text{C.32})$$

$$= \frac{1}{2} (1 \mp \frac{1}{d^2 - 1}) \mathbb{E}_{2:p} \langle \Phi_{\xi_{2:p}}(\mathbf{M}), \Phi_{\xi'_{2:p}}(\mathbf{M}) \rangle \quad (\text{C.33})$$

The sign of the second term depends on whether ξ_1 is 0 or 1, 2. Therefore the first moment of the Frobenius norm of $\Phi_\xi(\mathbf{M})$:

$$\mathbb{E}\langle \Phi_\xi(\mathbf{M}), \Phi_\xi(\mathbf{M}) \rangle \quad (\text{C.34})$$

$$= \frac{1}{2} (1 \pm \frac{1}{d^2 - 1}) \mathbb{E}_{2:p} \langle \Phi_{\xi_{2:p}}(\mathbf{M}), \Phi_{\xi_{2:p}}(\mathbf{M}) \rangle \quad (\text{C.35})$$

$$= (1 + O(pd^{-2})) \frac{\text{tr}(\mathbf{M}^2)}{2^p} \quad (\text{C.36})$$

Case 2: $\xi_1, \xi'_1 \in \{1, 2\}$ and $\xi_1 \neq \xi'_1$.

$$(C.26) \quad (C.37)$$

$$= \pm \mathbb{E} \langle \Phi_{\xi_{2:p}}(\mathbf{M}), \Phi_1^{(2)} \circ \Phi_{\xi'_{2:p}}(\mathbf{M}) \rangle \quad (C.38)$$

$$= \pm \frac{i}{2} \mathbb{E}_{2:p} \langle \Phi_{\xi_{2:p}}(\mathbf{M}), \quad (C.39)$$

$$\mathbf{H}_1 \Phi_{\xi'_{2:p}}(\mathbf{M}) - \Phi_{\xi'_{2:p}}(\mathbf{M}) \mathbf{H}_1 \rangle \quad (C.40)$$

$$= \pm \frac{i}{2} (\text{tr}(\Phi_{\xi'_{2:p}}(\mathbf{M}) \Phi_{\xi_{2:p}}(\mathbf{M})) \text{tr}(\mathbf{H}) \quad (C.41)$$

$$- \text{tr}(\Phi_{\xi_{2:p}}(\mathbf{M}) \Phi_{\xi'_{2:p}}(\mathbf{M})) \text{tr}(\mathbf{H})) \quad (C.42)$$

$$= 0 \quad (C.43)$$

Case 3: Either ξ_1 or $\xi'_1 = 0$ and $\xi_1 \neq \xi'_1$.

$$(C.26) \quad (C.44)$$

$$= \mathbb{E} \langle \Phi_{\xi_{2:p}}(\mathbf{M}), 0 \circ \Phi_{\xi'_{2:p}}(\mathbf{M}) \rangle \quad (C.45)$$

$$= 0 \quad (C.46)$$

Combining Case 2 and Case 3, $\mathbb{E} \langle \Phi_{\xi}(\mathbf{M}), \Phi_{\xi'}(\mathbf{M}) \rangle = 0$ for $\xi \neq \xi'$.

Second moments The correlation between the square of Frobenius norm can be calculated recursively as:

$$\mathbb{E} [\|\Phi_{\xi_{1:p}}(\mathbf{M})\|_F^2 \cdot \|\Phi_{\xi'_{1:p}}(\mathbf{M})\|_F^2] \quad (C.47)$$

$$= \mathbb{E} [\langle \Phi_{\xi_{1:p}}(\mathbf{M}), \Phi_{\xi_{1:p}}(\mathbf{M}) \rangle \quad (C.48)$$

$$\langle \Phi_{\xi'_{1:p}}(\mathbf{M}), \Phi_{\xi'_{1:p}}(\mathbf{M}) \rangle] \quad (C.49)$$

$$= \mathbb{E} \langle \Phi_{\xi_{2:p}}(\mathbf{M}) \Phi_l^{(0/1)} \circ \Phi_{\xi_{2:p}}(\mathbf{M}) \quad (C.50)$$

$$\cdot \langle \Phi_{\xi'_{2:p}}(\mathbf{M}) \Phi_l^{(0/1)} \circ \Phi_{\xi'_{2:p}}(\mathbf{M}) \rangle \quad (C.51)$$

$$= \frac{1}{4} \mathbb{E} [\|\Phi_{\xi_{2:p}}(\mathbf{M})\|_F^2 \cdot \|\Phi_{\xi'_{2:p}}(\mathbf{M})\|_F^2] \quad (C.52)$$

$$\pm \mathbb{E} [\text{tr}(\Phi_{\xi_{2:p}}(\mathbf{M}) \mathbf{H}_l \Phi_{\xi_{2:p}}(\mathbf{M}) \mathbf{H}_l) \|\Phi_{\xi'_{2:p}}(\mathbf{M})\|_F^2] \quad (C.53)$$

$$\pm \mathbb{E} [\|\Phi_{\xi_{2:p}}(\mathbf{M})\|_F^2 \text{tr}(\Phi_{\xi'_{2:p}}(\mathbf{M}) \mathbf{H}_l \Phi_{\xi'_{2:p}}(\mathbf{M}) \mathbf{H}_l)] \quad (C.54)$$

$$\pm \mathbb{E} [\text{tr}(\Phi_{\xi_{2:p}}(\mathbf{M}) \mathbf{H}_l \Phi_{\xi_{2:p}}(\mathbf{M}) \mathbf{H}_l) \quad (C.55)$$

$$\cdot \text{tr}(\Phi_{\xi'_{2:p}}(\mathbf{M}) \mathbf{H}_l \Phi_{\xi'_{2:p}}(\mathbf{M}) \mathbf{H}_l)] \quad (C.56)$$

$$= \frac{1 + O(d^{-2})}{4} \mathbb{E} [\|\Phi_{\xi_{2:p}}(\mathbf{M})\|_F^2 \cdot \|\Phi_{\xi'_{2:p}}(\mathbf{M})\|_F^2] \quad (C.57)$$

Therefore the diagonal elements of the Gram matrix has second moments:

$$\mathbb{E} [\|\Phi_{\xi_{1:p}}(\mathbf{M})\|_F^2 \cdot \|\Phi_{\xi_{1:p}}(\mathbf{M})\|_F^2] \quad (C.58)$$

$$= \frac{1 + O(d^{-2})}{4} \mathbb{E} [\|\Phi_{\xi_{2:p}}(\mathbf{M})\|_F^2 \cdot \|\Phi_{\xi_{2:p}}(\mathbf{M})\|_F^2] \quad (C.59)$$

$$= (1 + O(pd^{-2})) \frac{\text{tr}(\mathbf{M}^2)^2}{4p} \quad (C.60)$$

We are now ready to calculate the second moments for the off-diagonal elements of the Gram matrix. For $\xi, \xi' \in \Xi$:

$$\mathbb{E} \langle \Phi_{\xi_{l:p}}(\mathbf{M}), \Phi_{\xi'_{l:p}}(\mathbf{M}) \rangle^2 \quad (C.61)$$

$$= \mathbb{E} \langle \Phi_{\xi_{l+1:p}}(\mathbf{M}), (\Phi_l^{\xi_l})^* \circ \Phi_l^{\xi'_l} \circ \Phi_{\xi'_{l+1:p}}(\mathbf{M}) \rangle^2 \quad (C.62)$$

Case 1: $\xi_l = \xi'_l$.

$$(C.61) \quad (C.63)$$

$$= \mathbb{E} \langle \Phi_{\xi_{l+1:p}}(\mathbf{M}), \Phi_l^{(0/1)} \circ \Phi_{\xi'_{l+1:p}}(\mathbf{M}) \rangle^2 \quad (C.64)$$

$$= \frac{1}{4} \mathbb{E} [\text{tr}(\Phi_{\xi_{l+1:p}}(\mathbf{M}) \Phi_{\xi'_{l+1:p}}(\mathbf{M}))^2 \quad (C.65)$$

$$\pm 2 \text{tr}(\Phi_{\xi_{l+1:p}}(\mathbf{M}) \Phi_{\xi'_{l+1:p}}(\mathbf{M})) \quad (C.66)$$

$$\cdot \text{tr}(\Phi_{\xi_{l+1:p}}(\mathbf{M}) \mathbf{H}_l \Phi_{\xi'_{l+1:p}}(\mathbf{M}) \mathbf{H}_l) \quad (C.67)$$

$$+ \text{tr}(\Phi_{\xi_{l+1:p}}(\mathbf{M}) \mathbf{H}_l \Phi_{\xi'_{l+1:p}}(\mathbf{M}) \mathbf{H}_l)^2] \quad (C.68)$$

$$= \frac{1}{4} \left\{ \left(1 \pm \frac{2}{d^2 - 1}\right) \mathbb{E} [\text{tr}(\Phi_{\xi_{l+1:p}}(\mathbf{M}) \Phi_{\xi'_{l+1:p}}(\mathbf{M}))^2] \quad (C.69)$$

$$+ O(d^{-2}) \mathbb{E} [\|\Phi_{\xi_{l+1:p}}(\mathbf{M})\|_F^2 \cdot \|\Phi_{\xi'_{l+1:p}}(\mathbf{M})\|_F^2] \right\} \quad (C.70)$$

Case 2: $\xi_l, \xi'_l \in \{1, 2\}$ and $\xi_l \neq \xi'_l$. Up to a sign flip, we have

$$(C.61) \quad (C.71)$$

$$= \mathbb{E} \langle \Phi_{\xi_{l+1:p}}(\mathbf{M}), \Phi_l^{(2)} \circ \Phi_{\xi'_{l+1:p}}(\mathbf{M}) \rangle^2 \quad (C.72)$$

$$= -\frac{1}{4} \mathbb{E} [\langle \Phi_{\xi_{l+1:p}}(\mathbf{M}), \quad (C.73)$$

$$\mathbf{H}_l \Phi_{\xi'_{l+1:p}}(\mathbf{M}) - \Phi_{\xi'_{l+1:p}}(\mathbf{M}) \mathbf{H}_l \rangle^2] \quad (C.74)$$

$$= -\frac{1}{4} \mathbb{E} \{ \text{tr}(\Phi_{\xi'_{l+1:p}}(\mathbf{M}) \Phi_{\xi_{l+1:p}}(\mathbf{M}) \mathbf{H}_l)^2 \quad (C.75)$$

$$+ \text{tr}(\Phi_{\xi_{l+1:p}}(\mathbf{M}) \Phi_{\xi'_{l+1:p}}(\mathbf{M}) \mathbf{H}_l)^2 \quad (C.76)$$

$$- 2 \text{tr}(\Phi_{\xi_{l+1:p}}(\mathbf{M}) \Phi_{\xi'_{l+1:p}}(\mathbf{M}) \mathbf{H}_l) \quad (C.77)$$

$$\cdot \text{tr}(\Phi_{\xi'_{l+1:p}}(\mathbf{M}) \Phi_{\xi_{l+1:p}}(\mathbf{M}) \mathbf{H}_l) \} \quad (C.78)$$

$$= -\frac{1}{2(d-d-1)} \mathbb{E} [\text{tr}((\Phi_{\xi_{l+1:p}}(\mathbf{M}) \Phi_{\xi'_{l+1:p}}(\mathbf{M}))^2) \quad (C.79)$$

$$- \text{tr}(\Phi_{\xi_{l+1:p}}(\mathbf{M})^2 \Phi_{\xi'_{l+1:p}}(\mathbf{M})^2)] \quad (C.80)$$

$$\leq \frac{1}{d-d-1} \mathbb{E} [\text{tr}(\Phi_{\xi_{l+1:p}}(\mathbf{M})^2) \text{tr}(\Phi_{\xi'_{l+1:p}}(\mathbf{M})^2)] \quad (C.81)$$

Case 3: Either ξ_l or $\xi'_l = 0$ and $\xi_l \neq \xi'_l$. For the case where $\xi_l \neq \xi'_l$, and one of ξ_l and ξ'_l is 0, the correlation $\mathbb{E} \langle \Phi_{\xi_{l:p}}(\mathbf{M}), \Phi_{\xi'_{l:p}}(\mathbf{M}) \rangle^2 = 0$.

Combining the above three cases, we have the variance bounded:

$$\mathbb{V}(\langle \Phi_{\xi}(\mathbf{M}), \Phi_{\xi'}(\mathbf{M}) \rangle) = O(d^{-1}) \frac{\text{tr}(\mathbf{M}^2)^2}{4p} \quad (C.82)$$

□ $(k_1, k_2, \dots, k_p)^T \in \mathbb{Z}^p$, define:

D. Proofs for Upper Bounds

For any p -parameter quantum circuit of consideration, we can express the circuit as:

$$\mathbf{U}(\boldsymbol{\theta}) = \mathbf{V}_p(\theta_p)\mathbf{V}_{p-1}(\theta_{p-1}) \cdots \mathbf{V}_1(\theta_1), \quad (\text{D.1})$$

where $\mathbf{V}_l(\theta_l) = \exp(-i\theta_l \mathbf{H}_l)$ for some Hermitian \mathbf{H}_l . We can bound the number of local minima in $L(\boldsymbol{\theta}; \mathcal{S})$ depending the choice of $\{\mathbf{H}_l\}_{l=1}^p$. In this section, we provide a proof to Theorem 7 in Section 5:

Theorem 7 (Upper bound: the number of local minima). *Consider non-degenerated QNNs composed of unitaries generated by two-level Hamiltonians $\{H_l\}_{l=1}^p$ with p parameters. For training set \mathcal{S} , within each period, the loss function $L(\boldsymbol{\theta}; \mathcal{S})$ possesses at most $(4p)^p$ local minima.*

QNN with multi-qubit parameterized gates can have generating Hamiltonians $\{\mathbf{H}_l\}_{l=1}^p$ with more than two different eigenvalues. Specifically we consider Hamiltonians with integral eigenvalues $\{E_1, \dots, E_d\}$ such that $\max_{c,c'} |E_c - E_{c'}| \leq \Delta$. We can generalize Theorem 7 as:

Theorem 9 (An upper bound for the more general setting). *Consider p -parameter quantum neural networks composed of unitaries generated by Hamiltonians with integral spectrum gaps bounded by Δ . The loss function $L(\boldsymbol{\theta}; \mathcal{S})$ possesses at most $(4\Delta p)^p$ local minima, within each period, provided that the instance is not degenerated (i.e. the number of critical points is finite).*

Note that any Hamiltonians with rational eigenvalues are included with proper scaling and shifting.

In Subection D.1, we provide an upper bound on the Fourier degree of the loss function. In Subsection D.2, we bound the number of local minima for functions with bounded Fourier degree by considering the number of roots of a polynomial system.

D.1. Fourier Spectrum of the Loss Function

We first present a lemma on the Fourier spectrum of the loss function. For all $l \in [p]$, let $\{E_i^{(l)}\}_{i=1}^d$ be the integral eigenvalues for \mathbf{H}_l and let Δ_l denote the largest eigen-gap in absolute value: $\Delta_l := \max_{i,j \in [d]} |E_i^{(l)} - E_j^{(l)}|$. For arbitrary choice of training set \mathcal{S} , the loss function $L(\boldsymbol{\theta}; \mathcal{S})$ in Equation 5 has the following property:

Lemma 10 (Fourier Transformation of the loss function: Generalized version). *Let $\hat{L} : \mathbb{R}^p \rightarrow \mathbb{C}$ be the Fourier Transformation of $L(\boldsymbol{\theta}; \mathcal{S})$, namely for any $\mathbf{k} =$*

$$\hat{L}(\mathbf{k}) := \frac{1}{T_1 T_2 \cdots T_p} \int_{[0, T_1] \times \cdots \times [0, T_p]} L(\boldsymbol{\theta}; \mathcal{S}) \cdot \exp\left(-i \sum_{l=1}^p \frac{k_l \theta_l}{T_l}\right) d\boldsymbol{\theta} \quad (\text{D.2})$$

where T_l is the period of $L(\boldsymbol{\theta}; \mathcal{S})$ in θ_l . Let K be the support of \hat{L} (i.e. $K := \{\mathbf{k} \in \mathbb{R}^p | \hat{L}(\mathbf{k}) \neq 0\}$). The Fourier degree of the loss function $\Delta_K := \max_{\mathbf{k} \in K} \sum_{l=1}^p |k_l|$ is bounded by $\sum_{l=1}^p \frac{T_l \cdot \Delta_l}{\pi}$.

Proof. For all $l \in [p]$, let $\{\mathbf{u}_i^{(l)}\}_{i=1}^d$ be the eigenvectors of \mathbf{H}_l with corresponding eigenvalues $\{E_i^{(l)}\}_{i=1}^d$:

$$\mathbf{H}_l = \sum_{i=1}^d E_i^{(l)} \mathbf{u}_i^{(l)} \mathbf{u}_i^{(l)\dagger} \quad (\text{D.3})$$

The unitary gate parametrized by θ_l is therefore

$$\mathbf{V}_l(\theta_l) = \exp(-i\theta_l \mathbf{H}_l) = \sum_{i=1}^d e^{-i\theta_l E_i^{(l)}} \mathbf{u}_i^{(l)} \mathbf{u}_i^{(l)\dagger} \quad (\text{D.4})$$

And the unitary gate $\mathbf{U}(\boldsymbol{\theta})$ can be written as:

$$\mathbf{U}(\boldsymbol{\theta}) = \mathbf{V}_p(\theta_p)\mathbf{V}_{p-1}(\theta_{p-1}) \cdots \mathbf{V}_1(\theta_1) \quad (\text{D.5})$$

$$= \left(\sum_{i_p \in [d]} e^{-i\theta_p E_{i_p}^{(p)}} \mathbf{u}_{i_p}^{(p)} \mathbf{u}_{i_p}^{(p)\dagger} \right) \quad (\text{D.6})$$

$$\cdots \left(\sum_{i_1 \in [d]} e^{-i\theta_1 E_{i_1}^{(1)}} \mathbf{u}_{i_1}^{(1)} \mathbf{u}_{i_1}^{(1)\dagger} \right) \quad (\text{D.7})$$

$$= \sum_{\mathbf{i} \in [d]^p} \left(\prod_{l=1}^{p-1} \mathbf{u}_{i_{l+1}}^{(l+1)\dagger} \mathbf{u}_{i_l}^{(l)} \right) \left(\prod_{l=1}^p e^{-i \sum_{i=1}^p \theta_i E_{i_l}^{(l)}} \right) \quad (\text{D.8})$$

$$\cdot \left(\mathbf{u}_{i_p}^{(p)} \mathbf{u}_{i_1}^{(1)\dagger} \right) \quad (\text{D.9})$$

The output of the neural network given the density matrix ρ is therefore

$$f(\rho, \boldsymbol{\theta}) = \text{tr} \left(\mathbf{V}_p(\theta_p)\mathbf{V}_{p-1}(\theta_{p-1}) \cdots \mathbf{V}_1(\theta_1) \rho \right) \quad (\text{D.10})$$

$$\cdot \mathbf{V}_1(\theta_1)^\dagger \mathbf{V}_2(\theta_2)^\dagger \cdots \mathbf{V}_p(\theta_p)^\dagger \mathbf{M} \quad (\text{D.11})$$

$$= \sum_{\mathbf{i} \in [d]^p} \sum_{\mathbf{j} \in [d]^p} \hat{f}_{\mathbf{ij}}(\rho) \cdot e^{i \sum_{l=1}^p \theta_l (E_{j_l}^{(l)} - E_{i_l}^{(l)})} \quad (\text{D.12})$$

where for any $\mathbf{i}, \mathbf{j} \in [d]^p$

$$\hat{f}_{\mathbf{ij}}(\rho) = \left(\mathbf{u}_{i_1}^{(1)\dagger} \rho \mathbf{u}_{j_1}^{(1)} \right) \left(\mathbf{u}_{j_p}^{(p)\dagger} \mathbf{M} \mathbf{u}_{i_p}^{(p)} \right) \cdot \left(\prod_{l=1}^{p-1} \mathbf{u}_{i_{l+1}}^{(l+1)\dagger} \mathbf{u}_{i_l}^{(l)} \mathbf{u}_{j_l}^{(l)\dagger} \mathbf{u}_{j_{l+1}}^{(l+1)} \right) \quad (\text{D.13})$$

This indicates the Fourier coefficients of $f(\boldsymbol{\rho}; \boldsymbol{\theta})$ is supported on a subset of $\tilde{K} := \{(k_1, \dots, k_p) | \forall l \in [p], \exists i, j \in [d] : k_l = \frac{(E_i^{(l)} - E_j^{(l)})T_l}{2\pi}\}$, and that the Fourier degree of $f(\boldsymbol{\rho}, \boldsymbol{\theta})$ is bounded by $\sum_{l=1}^p \frac{T_l \Delta_l}{2\pi}$. Therefore for arbitrary $\boldsymbol{\rho}$ and label y , the Fourier degree of the square loss $(f(\boldsymbol{\rho}, \boldsymbol{\theta}) - y)^2$, $\Delta_K \leq \sum_{l=1}^p \frac{T_l \Delta_l}{\pi}$. Same holds for loss function $L(\boldsymbol{\theta}; \mathcal{S})$ with arbitrary training set \mathcal{S} . \square

For \mathbf{H}_l with integral eigenvalues,

$$\exp(-i(\theta_l + 2\pi)\mathbf{H}_l) \quad (\text{D.14})$$

$$= \sum_{i=1}^d e^{-i(\theta_l + 2\pi)E_i^{(l)}} \mathbf{u}_i^{(l)} \mathbf{u}_i^{(l)\dagger} \quad (\text{D.15})$$

$$= \exp(-i\theta_l \mathbf{H}_l). \quad (\text{D.16})$$

Hence $T_l \leq 2\pi$ and $\Delta_K \leq 2 \sum_{l=1}^p \Delta_l$. Let Δ be $\max_l \Delta_l$, the Fourier degree Δ_K of the loss function is bounded by $2\Delta p$.

For Hamiltonians with two-levels, we have the following corollary:

Corollary 11. *For quantum neural network instances composed of unitaries generated by two-level Hamiltonians, the Fourier degree of the loss function $L(\boldsymbol{\theta}; \mathcal{S})$ is bounded by $2p$ for arbitrary dataset \mathcal{S} .*

Proof. As shown earlier, for any Hermitian \mathbf{M} and for \mathbf{H}_l with the eigenvalues ± 1 , the output $f(\boldsymbol{\rho}, \boldsymbol{\theta})$ is periodic in π for each coordinate. Also notice for all $l \in [p]$, $\Delta_l = 2$. Hence the Fourier degree Δ_K of $L(\boldsymbol{\theta}; \mathcal{S})$ is bounded by $2p$. \square

D.2. Change of Variable and Root Counting

In this subsection, we elaborate on the change of variable and the upper bound on number of critical points by Bézout's Theorem. This would complete our proof for Theorem 7 and 9.

Let T_l be the period of $L(\boldsymbol{\theta}; \mathcal{S})$ in θ_l , and $\hat{L}(\mathbf{k})$ the Fourier coefficient for $\mathbf{k} = (k_1, \dots, k_p)^T \in \mathbb{Z}^p$. We have

$$L(\boldsymbol{\theta}; \mathcal{S}) = \sum_{\mathbf{k} \in K} \hat{L}(\mathbf{k}) \left(\cos \frac{k_1 \theta_1}{T_1} + i \sin \frac{k_1 \theta_1}{T_1} \right) \cdots \left(\cos \frac{k_p \theta_p}{T_p} + i \sin \frac{k_p \theta_p}{T_p} \right) \quad (\text{D.17})$$

Here $K \subseteq \mathbb{Z}^p$ is the support of the Fourier coefficients.

By definition, a local minimum must be a critical point, hence it suffices to bound the number of critical points for

$L(\boldsymbol{\theta}; \mathcal{S})$. Define $G_l(\boldsymbol{\theta})$ as

$$G_l(\boldsymbol{\theta}) = \frac{\partial}{\partial \theta_l} L(\boldsymbol{\theta}; \mathcal{S}) \quad (\text{D.18})$$

$$= \sum_{\mathbf{k} \in K} k_l \hat{L}(\mathbf{k}) \left(-\sin \frac{k_l \theta_l}{T_l} + i \cos \frac{k_l \theta_l}{T_l} \right) \quad (\text{D.19})$$

$$\cdot \prod_{l' \neq l} \left(\cos \frac{k_{l'} \theta_{l'}}{T_{l'}} + i \sin \frac{k_{l'} \theta_{l'}}{T_{l'}} \right) \quad (\text{D.20})$$

We can tell from above expression that the Fourier spectrum of G_l is supported on the same set K . A critical point of $L(\boldsymbol{\theta}; \mathcal{S})$ must satisfies that for all $l \in [p]$, $G_l(\boldsymbol{\theta}) = 0$.

By induction, $\cos k\theta$ can be expressed as a degree- k polynomial of $\cos \theta$ and $\sin k\theta$ as a degree- $(k-1)$ polynomial of $\cos \theta$ multiplied by $\sin \theta$. Consider the change of variable

$$c_l = \cos(\theta_l/T_l), \quad s_l = \sin(\theta_l/T_l), \quad \forall l \in [p]. \quad (\text{D.21})$$

Let $g_l(c_1, s_1, \dots, c_p, s_p)$ be the multivariate polynomial constraints corresponding to $G_l(\boldsymbol{\theta})$ after the change of variable:

$$\sum_{\mathbf{k} \in K} k_l \hat{L}(\mathbf{k}) \left(-s_l U_{k_l-1}(c_l) + i T_{k_l}(c_l) \right) \cdot \prod_{l' \neq l} \left(T_{k_{l'}}(c_{l'}) + i s_{l'} U_{k_{l'}-1}(c_{l'}) \right) \quad (\text{D.22})$$

where $T_k(\cdot)$ and $U_k(\cdot)$ are Chebyshev polynomials of the first and second kind. For each g_l , the sum of degrees of $c_{l'}$ and $s_{l'}$ is bounded by $\max_{\mathbf{k} \in K} |k_{l'}|$, and the degree $\deg(g_l)$ of g_l is bounded by $\Delta_K = \max_{\mathbf{k} \in K} \sum_{l=1}^p |k_l|$. The change of variable is one-to-one from $\theta_l \in [0, T_l)$ to a pair of $(c_l, s_l) \in \mathbb{R}^2$ under the constraint $c_l^2 + s_l^2 = 1$. Therefore, it suffices to count the number of roots of the polynomial system with $2p$ parameters and $2p$ constraints:

$$\begin{cases} g_1(c_1, s_1, \dots, c_p, s_p) = 0, \\ \vdots \\ g_p(c_1, s_1, \dots, c_p, s_p) = 0, \\ h_1(c_1, s_1, \dots, c_p, s_p) = c_1^2 + s_1^2 - 1 = 0, \\ \vdots \\ h_p(c_1, s_1, \dots, c_p, s_p) = c_p^2 + s_p^2 - 1 = 0. \end{cases} \quad (\text{D.23})$$

Notice that for general polynomial system, the number of critical points can be unbounded. For example, consider a system composed of constant polynomials, every point in the domain is a critical point. This corresponds to constant loss function, where the gradients vanishes everywhere with positive semidefinite Hessians. For this reason, we will focus on the non-degenerated case with finitely many critical points. Under the premise of non-degeneracy, Bézout's

Theorem (e.g. Section 3.3 in (Cox et al., 2006)) states that the number of roots can be bounded by the product of degree of polynomial constraints $2^p \deg(g_1) \deg(g_2) \cdots \deg(g_p) \leq (2\Delta_K)^p$.

We also prove a similar result for the more general case where the generators are Hamiltonians with integral spectrum: let Δ be the largest eigen-gap for each of the Hamiltonians, the number of local minima within each period is upper bounded by $O((\Delta p)^p)$. Combined with results in Subsection D.1, the proof for Theorem 7 and 9 is complete.

E. Numerical Results

For all the experiments in this section, we study the p -parameter QNN as mentioned in Example 1 in S.M. Sect. B, where :

$$\mathbf{M} := \otimes_{l=1}^p (\mathbf{Y} + \mathbf{I}) \quad (\text{E.1})$$

$$\mathbf{H}_l := \left(\otimes_{r=1}^{l-1} \mathbf{I} \right) \otimes \mathbf{Z} \otimes \left(\otimes_{l+1}^p \mathbf{I} \right), \quad \forall l \in [p] \quad (\text{E.2})$$

In S.M. Sect. E.1, we provide details and more numerical results for experiments described in Section 6. In S.M. Sect. E.2, we visualize the 2-d loss landscape of Example 3.

E.1. Training with Gradient-based Methods

In this subsection, we use Example 2 to demonstrate that our construction can be hard to train with *gradient-based methods*. The loss function of the example can be expressed as

$$\frac{1}{2p} \sum_{l=1}^p \left((\sin 2\theta_l - \sin \frac{\pi}{50})^2 + \frac{1}{4} (\cos 2\theta_l - \cos \frac{\pi}{50})^2 \right). \quad (\text{E.3})$$

with global minima at $\theta^* = \left(\frac{\pi}{100}, \dots, \frac{\pi}{100} \right)^T$.

Hyperparameters. For all three optimizers, we choose the (initial) learning rate to be 0.01. For RMSProp, we choose the smoothing constant α for mean-square estimation to be 0.99. For Adam, we set the averaging coefficients $\beta_1 = 0.9$ for the gradients and $\beta_2 = 0.999$ for its square. For L-BFGS we choose the history size to be 100. The numbers of iterations for training are set to 200-th for each pair of instances and optimizers; as can be seen in Figure 6, all pairs have already converged at the 100-th iteration.

Training curves We plot the training curve for QNN instances with 2, 4, 8, 16 and 32 parameters with Adam, RMSProp and L-BFGS. For each pair of instance and optimizer, we repeat the experiments with uniform random initialization. As shown in Figure 6, for all the experiment

setting considered here, while all initialization converge efficiently, there are initializations that does not converge to the global minima.

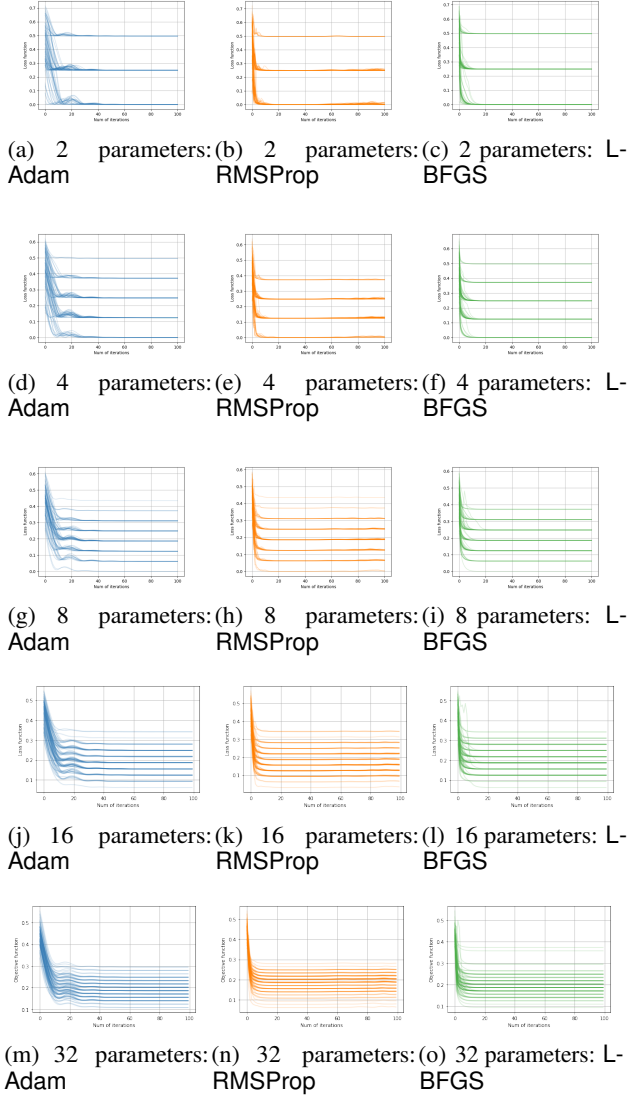
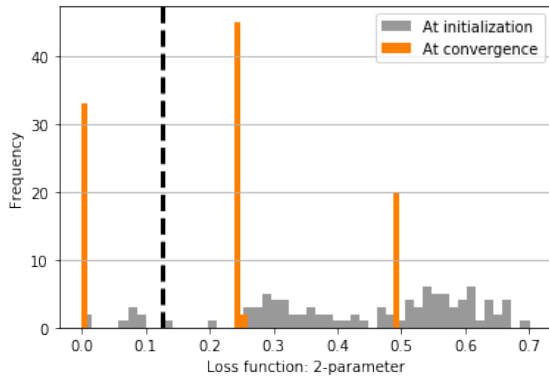


Figure 6. Empirical risk minimization of different QNN instance with Adam, RMSProp and L-BFGS. For each experiment setting we repeat 100 times.

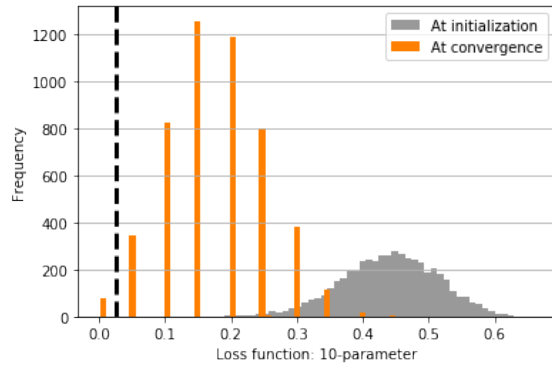
More on distributions of function values In Figure 7, we plot more results on the distribution of function values under RMSProp and have similar observation as mentioned in Section 6.

Calculating the empirical probabilities For all the instances of consideration, the function values of local minima can be calculated. For p -parameter instances, the function value of global minima is 0, and for the other local minima,

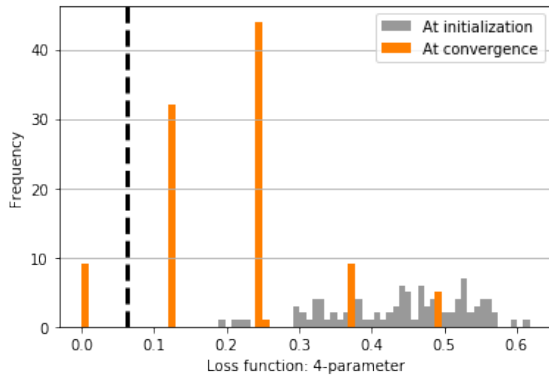
Exponentially Many Local Minima in Quantum Neural Networks



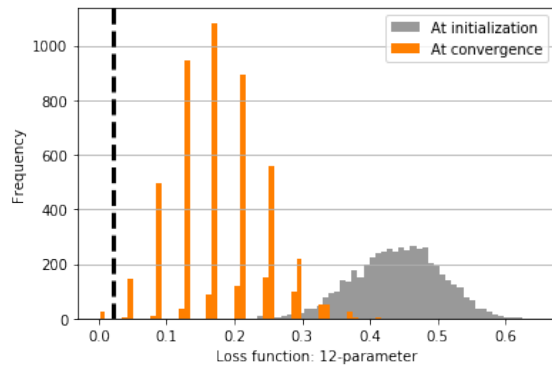
(a) 2 parameters: RMSProp



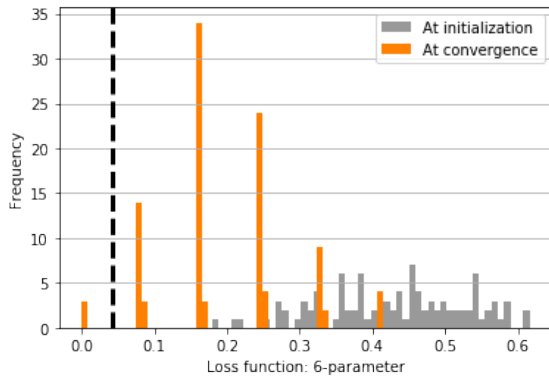
(e) 10 parameters: RMSProp



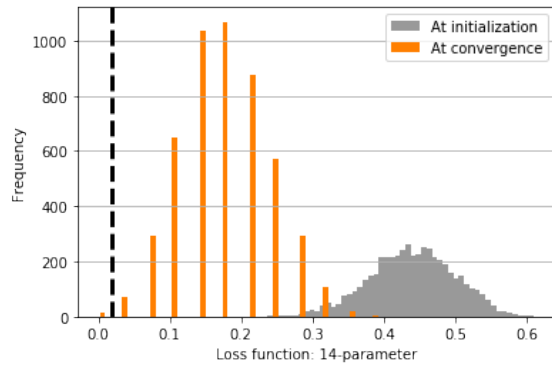
(b) 4 parameters: RMSProp



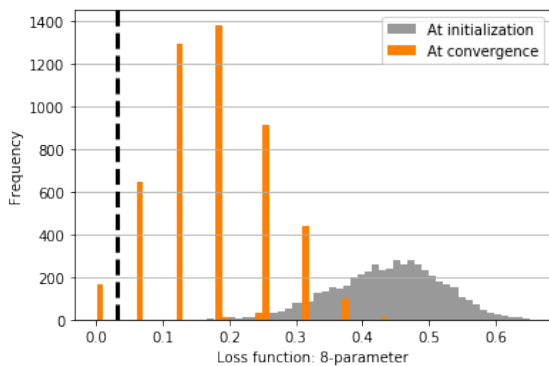
(f) 12 parameters: RMSProp



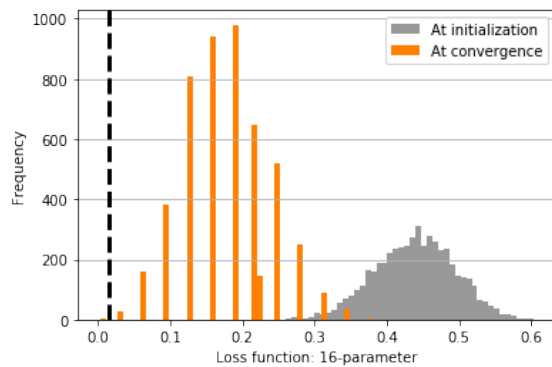
(c) 6 parameters: RMSProp



(g) 14 parameters: RMSProp



(d) 8 parameters: RMSProp



(h) 16 parameters: RMSProp

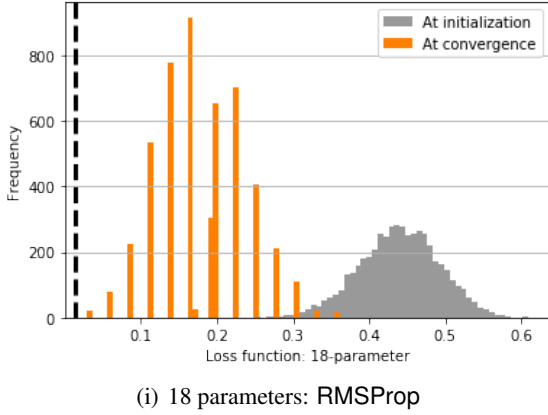


Figure 7. Distribution of function values of QNN instances with RMSProp. For instances with size 2, 4, 6, the experiments are repeated 200 times; for the rest of the instances, the experiments are repeated 5000 times.

the function values are at least $0.5/p$. For calculating the empirical probability that random initialization converges to the global minima, we count the number of trial that converge to values less than $0.25/p$.

E.2. Visualization: Non-decomposable Construction

For low-dimensional cases, it is possible to visualize the loss function of Example 3 of the construction by plotting the contour of the landscape. In Figure 8, we plot the contour of our construction for $p = 2$, with loss function proportional to

$$\begin{aligned} & (\sin 2\theta_1 - \sin \frac{\pi}{50})^2 + (\sin 2\theta_2 - \sin \frac{\pi}{50})^2 \\ & + \frac{1}{16} ((\cos 2\theta_1 - \cos \frac{\pi}{50})^2 + \frac{3}{2} (\cos 2\theta_2 - \cos \frac{\pi}{50})^2) \\ & + \frac{1}{8} (\cos 2\theta_1 \cos 2\theta_2 - \cos^2 \frac{\pi}{50})^2 \quad (\text{E.4}) \end{aligned}$$

The global minima are $(k_1\pi + \frac{\pi}{100}, k_2\pi + \frac{\pi}{100})$ with $k_1, k_2 \in \mathbb{Z}$. Within each period, there are a total of 4 local minima where black box local search methods might stuck at. Among them, the global minima are marked in black. The gradient-based methods only converge to the global minimum when the initial value of the parameter lies in certain region.

E.3. Robustness of the Constructions

Our construction above demonstrates that in the worst-case, under-parameterized QNNs can have exponentially many local minima. It is natural to ask whether the local minima in our constructions are stable under perturbation. To this end, we repeated our experiments with Gaussian noises $\mathcal{N}(0, \sigma)$ added to the labels. The function values at local minima, as shown in Figure 9(a) (Cf. Figure 2,3 in the

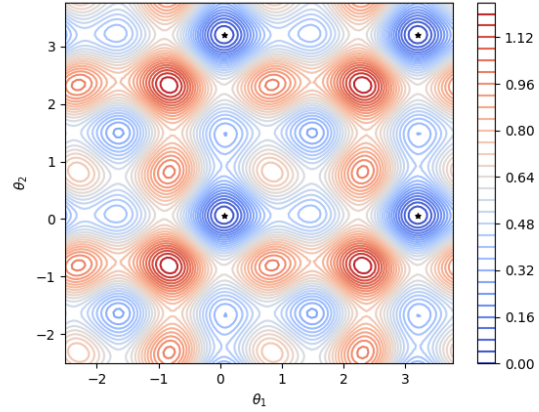


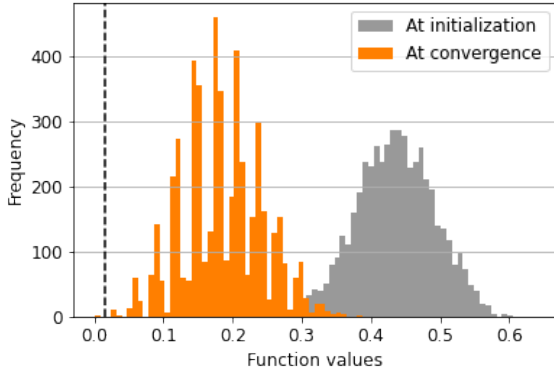
Figure 8. Landscape of the constructed QNN instance with 2 qubits and 2 parameters. The global optima are marked in black.

main text and Figure 7(h) in the supplementary material), have changed, as the noise breaks the symmetry of suboptimal minima. But as shown in Figure 9(b) (Cf. Figure 4 in the main text), the exponential decay of success rate in finding the global minima remains for different σ (recall that the labels in our construction are in $[0, 1]$). We used RMSProp optimizer, with other hyperparameters the same as the pervious experiments.

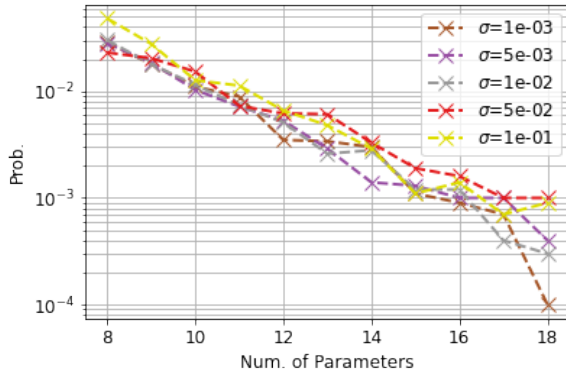
Moreover, by direct calculation of the suboptimality gaps and eigenvalues of Hessians at local minima, it can be proved that our examples are indeed robust against random label perturbations, quantum noise due to noisy gates, or due to the finite number of measurements, and even **adversarial** perturbations, as long as the resulting perturbation in the loss function is bounded in ℓ_∞ -norm.

E.4. More Experiments on Datasets beyond Our Construction

So far we have observed exponentially many local minima in the datasets in our construction. Now we turn to more natural datasets that may appear in practice. Specifically, we consider the following family of datasets with a clear interpretation as an encoding of a classical, linearly separable concept: for the p -parameter instance, we first randomly choose $\mathbf{w} \in \mathbb{R}^{2p}$ as the normal vector to the separating hyperplane. The classical dataset $\{(\mathbf{x}, y) | \mathbf{x} \in \mathbb{R}^{2p}, y \in \{0, 1\}\}$ is generated as follows: (1) uniformly draw the feature vector $\mathbf{x} = (x_1, \dots, x_p, x_{p+1}, \dots, x_{2p})^T$ from $[0, 2\pi]^{2p}$; (2) $y = 1$ if $\mathbf{w}^T \mathbf{x} > 0$ and $y = 0$ otherwise. The classical feature \mathbf{x} is encoded into a quantum state $\rho(\mathbf{x}) = |\Psi(\mathbf{x})\rangle \langle \Psi(\mathbf{x})|$ using the two-layer XY-encoder: $\Psi(\mathbf{x}) := \otimes_{l=1}^p \exp(-ix_{p+l} \mathbf{Y}_l) \otimes_{l=1}^p \exp(-ix_l \mathbf{X}_l) |0\rangle^{\otimes p}$.



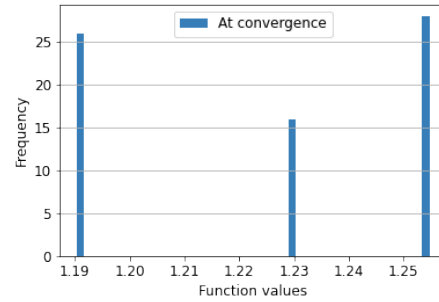
(a) Function values at initialization and at convergence for the 16-parameter instance with noisy labels, repeated for 5000 random initializations.



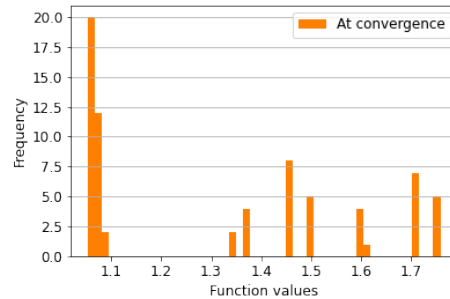
(b) The exponential decay of success rate for finding the global minimum under 10000 random initialization with label noise $\mathcal{N}(0, \sigma)$.

Figure 9. Empirical risk minimization with noisy labels. (a) the function values at convergence for a 16-parameter instance; the perturbation breaks the symmetry of the local minima, hence the more continuous spectrum of function values (Cf. Figure 3(h)). (b) the decay of success rate for finding the global minima; the exponential tendency remains in the presence of Gaussian label noise up to $\sigma = 1e - 1$.

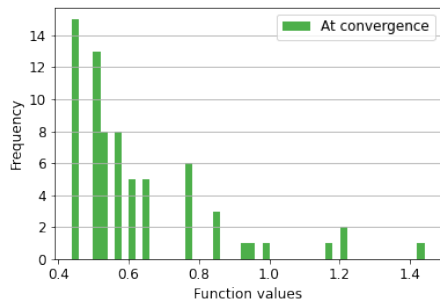
This process is repeated to construct a 100-sample dataset. For each QNN instance, we sampled 70 initial points and optimize the mean-square loss with RMSProp for 2000 iterations. The rest of the settings are the same as our original experiments. In Figure 10 (Cf. Figure 3 in the main text and Figure 7 (a)-(d) in the supplementary material), we trained instances with 2,4,6,8 qubits, each with 70 random initialization, and plotted the distribution of function values at convergence. There is a large number of local minima, and only a few random initialization ended up at the global minima. While we no longer have a clear exponential dependency, we did observe that as the number of parameters increases, the number of local minima increases significantly, and the success rate for finding global minima drops sharply. Such a phenomenon is also resilient to random choices of w and random sampling of feature vectors. This could be initial numerical evidence supporting the generality of our observed phenomena.



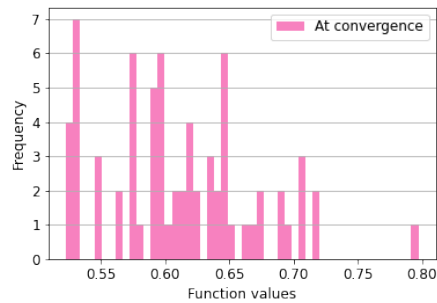
(a) 2 parameters: RMSProp



(b) 4 parameters: RMSProp



(c) 6 parameters: RMSProp



(d) 8 parameters: RMSProp

Figure 10. Empirical risk minimization for the common dataset using RMSProp. For each experiment setting, we repeat for 70 random initializations and run for 2000 iterations. The number of local minima increases significantly with the number of parameters.